

LAPPEENTANTA UNIVERSITY OF TECHNOLOGY

FACULTY OF TECHNOLOGY

Master's Degree Programme in Technomathematics and Technical Physics

Leonid Patrikeev

**STRUCTURAL MODELLING OF LIQUID ZrO_2 AND GLASSY B_2O_3
BY USING AB INITIO MOLECULAR DYNAMICS METHOD .**

Examiners: Professor Erkki Lähderanta

Ph.D Jaakko Akola

ABSTRACT

Lappeenranta University of Technology
Faculty of Technology
Master's Degree Programme in Technomathematics and Technical Physics

Leonid Patrikeev

Structural modelling of liquid ZrO₂ and glassy B₂O₃ by using AB INITIO Molecular Dynamics method

Master's thesis

2012

73 pages, 23 figures, 9 tables

Examiners:

Professor Erkki Lähderanta

Ph.D. Jaakko Akola

Keywords: AB INITIO, molecular Dynamics, atomic structure, B₂O₃, diboron trioxide, ZrO₂, zirconium dioxide, computer simulation, DFT theory, fractional number, Monte Carlo method.

Atomic structure of ZrO₂ and B₂O₃ was investigated in this work. New data under extreme conditions ($T = 3100$ K) was obtained for the liquid ZrO₂ structure. A fractional number of boron was investigated for glassy structure of B₂O₃. It was shown that it is possible to obtain an agreement for the fractional number between NMR and DFT techniques using a suitable initial configuration.

Acknowledgments

I am very thankful to Professor Erkki Lähderanta for giving me an opportunity to study in Lappeenranta University of Technology.

I wish to express my gratitude to Jaakko Akola for supervising me and for helpful discussions during this work.

I am also very grateful to Shinji Kohara (Spring-8, Tokyo, Japan) for preparation of X-ray diffraction measurements and valuable comments concerning this work.

List of symbols

ρ electronic density

φ_i one-particle wavefunction for an electron

H_e Hamiltonian for an electronic system

φ_o wavefunction for an electronic ground state

Ψ_k wavefunction for an excited electronic state

D_i^{kk} diagonal correction terms

L Lagrangian for an electronic system

Λ_{ij} Lagrangian multipliers

H_e^{HF} effective one-particle Hamiltonian of Hartree-Fock

R_i position of nuclei

L_{cp} Lagrangian of Car-Parrinello

μ fictitious mass of electron

ε_i eigenvalue of wavefunction for a certain orbital

E_{gap} energy gap

E_{cut} largest kinetic energy in an expansion of the wavefunction in terms of a plane wave basis set

Δt^{max} maximal time step

T_e fictitious electronic kinetic energy

E^{ks} Kohn-Sham energy

n charged density

T_s kinetic energy of a non-interacting reference system

V_{ext} external potential

V_H Hartree potential

$E_{xc}[n]$ exchange-correlation functional

V^{KS} local potential

H_e^{KS} one-particle Hamiltonian of Kohn-Sham

E_{xc} exchange-correlation energy

ζ coulomb operator

K exchange operator

f_m^S Slater-type basis function

f_m^G Gaussian-type basis function

f_G^{PW} plane Waves-type basis function

G vector in reciprocal space

f_G^{GPW} Generalized Plane Waves-type basis function

g_{ij} Riemannian metric tensor

V^{PP} norm-conserving pseudopotential

Y_{lm} spherical harmonics

ΔV_{local} local part of pseudopotential potential

ΔV_{core} 'core' part of pseudopotential

P_k projector

S_I structure factor

j_l spherical Bessel functions of the first kind

l_m angular momentum quantum number

ρ_i spin density

ε_c correlation functional

ε_x exchange functional

ΔE_C^{GG} correction of the gradient correlation functional

χ^2 difference between the measured total structure factor and determined from the configuration

Achronyms

HF Hartree-Fock

KS Kohn-Sham

CP Car-Parrinello

DFT Density Functional Theory

BO Born-Oppenheimer

EXT External

STOs Slater-type basis functions

GTOs Gaussian-type basis functions

LCAO Linear Combination of Atomic Orbitals

PW Plane Waves

GPW Generalized Plane Waves

LDA Local Density Approximation

LSDA Local Spin Density Approximation

PW Perdew and Wang

VWN Vosko, Wilk and Nusair

GGA Generalized Gradient Approximation

LYP Correlation functional of Lee, Yang and Parr

RMC Reverse Monte Carlo

MD Molecular Dynamics

XRD X-Ray diffraction

HOMO Highest Energy Occupied Molecular Orbital

LUMO Lowest energy Unoccupied Molecular Orbital

f fractional number for boron in boroxol rings

PDOS Projected density of states

BFGS Broyden–Fletcher–Goldfarb–Shanno

Table of contents

Introduction	11
1. Used methods	12
1.1 The basic definitions of DFT methods	12
1.2 Ab Initio Molecular Dynamic Method	13
1.2.1 Born-Oppenheimer Molecular Dynamics	13
1.2.2 Car-Parrinello Molecular Dynamics	15
1.2.2.1 Introduction to the method	15
1.2.2.2 Car-Parrinello Lagrangian and Equations of Motion	16
1.2.2.3 How to Control Adiabaticity?	18
1.2.2.4 The Quantum Chemistry Viewpoint.....	19
1.3 Electronic Structure Methods	20
1.3.1 Density Functional Theory	20
1.3.2 How to solve Kohn-Sham equations?	24
1.3.3 Hartree-Fock Theory	25
1.3.4 Comparison between Hartree-Fock and Kohn-Sham methods	26
1.3.5 Basis Sets	27
1.3.5.1 Gaussians and Slater Functions	27
1.3.5.2 Plane Waves	28
1.3.6. Pseudopotentials	29
1.3.7 Exchange and correlation in DFT.....	30
1.3.7.1. The Local Density Aproximation (LDA)	31
1.3.7.2 The generalized gradient approximation (GGA).....	32
1.3.7.3. Hybrid HF-KS approaches	34
1.4.1. Reverse Monte Carlo Modelling	35
1.5 Classical methods of computer modelling.....	38
1.5.1 Classical Monte Carlo method	38
1.5.2 Classical molecular dynamics method	39
2. Experiment	40
2.1 Calculation software	40

2.2.1 Atomic structure of ZrO ₂ (DFT MD simulation)	40
2.2.2 Atomic structure of ZrO ₂ (CLASSICAL MD simulation)	51
2.3 Atomic structure of glassy B ₂ O ₃	51
2.3.1 Ab initio MD simulation using initial configurations after RMC refinement.....	51
2.3.2. Preparation of initial configurations by using classical MC method	55
2.3.3 Creation of initial configuration using both methods (RMC and Classical MC).....	58
2.3.4 Projected density of states for boroxol-rich B ₂ O ₃ structure.	59
2.3.5. Comparison between boroxol-rich and boroxol-poor structures.....	60
Conclusion	64
References	65
Appendix 1. The input file for the cp2k program. Ab initio MD simulation of glassy B ₂ O ₃ structure (Microcanonical ensemble).	68
Appendix 2. The input file for the cp2k program. Ab initio MD simulation of liquid ZrO ₂ structure (Canonical ensemble).	71

Introduction

"Traditional" methods of quantum chemistry, based on the Hartree-Fock approximation as a starting point and using the idea of the wave function as the characteristics of a quantum system, in principle, can provide an accurate answer about the structure, energy, and chemical properties for any material. This requires a full accounting of the exchange and correlation energies between electrons and a full basis set for atomic orbitals which do not contain errors. Currently, such calculations are possible only for very simple molecules. Even the most successful approaches are applicable to molecular systems containing only ca. 10 heavy atoms.

A very attractive alternative to these methods is density functional theory (DFT). It was found that DFT methods, in spite of sometimes very rough approximations, in many cases, provide the same results (or even exceeding the accuracy) as the methods based on Hartree-Fock calculations. Not surprisingly, the best DFT methods have become more popular than Hartree-Fock methods.

The main purpose of this paper is structural modelling of liquid ZrO_2 and B_2O_3 using DFT calculations. In most cases, we used synchrotron x-ray diffraction (XRD) measurement (Spring-8, Japan) to create the initial configurations using the reverse Monte Carlo method.

Zirconium dioxide is a well-studied material. However, we investigated the atomic structure under the extreme temperature ($T = 3100$ K). Currently, there is no information about structure of ZrO_2 at such high temperatures. Therefore, our investigation can be considered as a new.

There are several articles about the structure of B_2O_3 based on DFT methods. However, the investigated systems in these articles are small (approximately 100 atoms). In addition, there is no agreement in the literature for fractional number of boron (f) using various techniques ($f \leq 0.3$ in case of DFT simulation; $f \approx 0.7$ using nuclear magnetic resonance measurements). Therefore, an important aim is to establish the fractional number for boron.

1. Used methods

1.1 The basic definitions of DFT methods

Let us give several definitions. Function is a correspondence to a series of numbers to another one, i.e., function "takes" a number and "returns" another number, which is associated with first one: $y = f(x)$. The functional associates the number and function, which is compared to another number, i.e. $y = F[f(x)]$, or simply $y = F[f]$. One can carry out the same operations with a functional, as with a function (for example, to differentiate):

$$\begin{aligned}\delta F[f] &= F[f + \delta f] - F[f] = \int \frac{\delta F}{\delta f(x)} \delta f(x) dx \\ \frac{\delta}{\delta f(x)} (F_1 F_2) &= \frac{\delta F_1}{\delta f(x)} (F_2) + \frac{\delta F_2}{\delta f(x)} (F_1)\end{aligned}\quad (1)$$

The main physical variable for DFT methods is the electron density ρ . This is a function of all electronic coordinates which are included in a system.

For a single electron using Hartree-Fock methods we have the following expression:

$$\rho_i(r) = |\varphi_i(r)|^2 \quad (2)$$

where $\varphi_i(r)$ is a one-particle wavefunction for an electron. The total electron density produced by all electrons of the molecule is equal to:

$$\rho_{total}(r) = \sum_{i=1}^N |\varphi_i(r)|^2 \quad (3)$$

For many years, the usage of electron density to describe the quantum system was more intuitive than rigorously proven. The electron density is much more attractive than the wave function. First of all, the electron density is physically defined and, in principle, measurable in contrast to the wave function, which has no physical meaning. Second, the wave function of the N-electron system depends on the 3N coordinates of the electrons (or even 4N, if we take into account the spin), whereas the electron density is always a function of three coordinates independently of the number of electrons in the molecule.

In 1964, Hohenberg and Kohn proved the theorem that properties of the ground state are a functional of the electron density ρ . It was the second birth of DFT methods. According to the theorem of Hohenberg and Kohn, the energy of the ground state of the molecule is a functional of the electron density. The energy is minimal, if ρ is an electron density for the ground state [1].

1.2 Ab Initio Molecular Dynamic Method

There are two main techniques for *ab initio* molecular dynamic simulation: Born-Oppenheimer and Car-Parrinello methods. Both techniques have been fully described in the review of D. Marx and Jurg Hutter “Ab Initio Molecular Dynamic: Theory and implementation, John von Neiman Institute for Computing, 2000” [2]. We use their description for the explanation of these modeling techniques.

1.2.1 Born-Oppenheimer Molecular Dynamics

The most common approach to include the electronic structure in molecular dynamics simulation is to solve the problem of static electronic structure of molecular dynamics at each step, given the set of fixed nuclear positions for each time interval. In such a way, the electronic part of the structure is reduced to solving the time-independent quantum problem, for example, by solving the time-independent Schrödinger equation, while the nuclei are treated by means of classical molecular dynamics. Therefore, the time dependence of the electronic structure is the result of motion of the nuclei. As a result of the Born-Oppenheimer molecular dynamics method can be defined as:

$$M_I \ddot{\mathbf{R}}_I(t) = -\nabla_I \min_{\Psi_0} \{ \langle \Psi_0 | \mathcal{H}_e | \Psi_0 \rangle \} \quad (4)$$

$$E_0 \Psi_0 = \mathcal{H}_e \Psi_0 \quad (5)$$

for the electronic ground state [2].

It is also possible to apply the same scheme of Born-Oppenheimer molecular dynamics for excited electronic states Ψ_k without considering any interference effects; in particular, this means that the diagonal terms should be equal to zero (see the equation 6):

$$D_I^{kk}(\{\mathbf{R}_I(t)\}) = - \int d\mathbf{r} \Psi_k^* \nabla_I^2 \Psi_k \quad (6)$$

These terms of renormalization for Born-Oppenheimer MD or "adiabatic approximation" for the nuclei of this state Ψ_k (which can also be the ground state Ψ_0) and lead to the so-called "adiabatic potential" of this state.

It is advisable to formulate the BO equations of motion for the special case of effective one-particle Hamiltonians. This may be the Hartree-Fock approximation which can be defined as the variational minimum of energy expectation value $\langle \Psi_0 | H_e | \Psi_0 \rangle$ that gives a single Slater determinant $\Psi_0 = \det\{\psi\}$ with the constraints that the single-particle orbitals ψ are orthonormal:

$$\langle \psi_i | \psi_j \rangle = \delta_{ij} \quad (7)$$

Restrictions for energy minima can be written as

$$\min_{\{\psi_i\}} \{ \langle \Psi_0 | \mathcal{H}_e | \Psi_0 \rangle \} \Big|_{\{\langle \psi_i | \psi_j \rangle = \delta_{ij}\}} \quad (8)$$

which leads us to the Lagrangian formalism

$$\mathcal{L} = - \langle \Psi_0 | \mathcal{H}_e | \Psi_0 \rangle + \sum_{i,j} \Lambda_{ij} (\langle \psi_i | \psi_j \rangle - \delta_{ij}) \quad (9)$$

where Λ_{ij} are the associated Lagrangian multipliers. Unconstrained variation of this Lagrangian with respect to the orbitals

$$\frac{\delta \mathcal{L}}{\delta \psi_i^*} \stackrel{!}{=} 0 \quad (10)$$

leads to the well-known Hartree-Fock approximation

$$\mathcal{H}_e^{\text{HF}} \psi_i = \sum_j \Lambda_{ij} \psi_j \quad (11)$$

the diagonal canonical form $H_e^{HF} \psi_i = \epsilon \psi_i$ can be found by a unitary transformation and H_e^{HF} is an effective single-particle Hamiltonian. Therefore, the equations of motion can be written as

$$M_I \ddot{\mathbf{R}}_I(t) = -\nabla_I \min_{\{\psi_i\}} \{ \langle \Psi_0 | \mathcal{H}_e^{HF} | \Psi_0 \rangle \} \quad (12)$$

$$0 = -\mathcal{H}_e^{HF} \psi_i + \sum_j \Lambda_{ij} \psi_j$$

for the Hartree-Fock case [2] .

A similar system of equations can be written if Hohenberg-Kohn-Sham density functional theory is used, where H_e^{HF} should be replaced by the Kohn-Sham effective single-particle Hamiltonian H_e^{KS} .

Instead of diagonalizing the single-particle Hamiltonian, an equivalent approach is to perform the minimization procedure according to the equation (8) using nonlinear optimization techniques.

Early applications of the Born-Oppenheimer molecular dynamics were carried out in the semi-empirical approach to the problem of electronic structure. Born-Oppenheimer dynamics started to become very popular in the early nineties with the emergence of more efficient electronic structure codes in combination with sufficient computer power to solve some "interesting tasks" [2].

1.2.2 Car-Parrinello Molecular Dynamics

1.2.2.1 Introduction to the method

The second widespread approach to cut down the computational expenses of molecular dynamics which includes the electrons in a single state was proposed by Car and Parrinello in 1985. Molecular dynamics of Car-Parrinello was formulated in the framework of an alternative formalism of classical mechanics, namely using a formalism of Lagrange. Using this formalism, it is possible to separate the electronic and nuclear degrees of freedom. Moreover, there is no electron dynamics whatsoever involved in solving the Born-Oppenheimer (see equations (4) and (5)), i.e. they can be integrated on the time scale given by

nuclear motion. However, this means that the electronic structure problem has to be solved self-consistently at each molecular dynamics step.

In conclusion, this method allows to integrate the equations of motion on the (long) time scale set by the nuclear motion, but nevertheless taking into account the evolution of the electronic subsystem as much as possible. The second point allows to circumvent explicit diagonalization or minimization to solve the problem of electronic structure for the next step of molecular dynamics [2].

1.2.2.2 Car-Parrinello Lagrangian and Equations of Motion

The main idea of the Car-Parrinello approach can be considered for a quantum-mechanical adiabatic time scale separation of fast electronic and slow nuclear motions, turning it into classical mechanical adiabatic energy scale separation in the framework of the well-known theory of dynamical systems. To achieve this goal a two-component quantum (for nuclei and electrons motions), the problem is decomposed into two components of the classical problem with two separate energy scales at the expense of an explicit time dependence of the quantum dynamics of the subsystem. In addition, the energy of the electron subsystem $\langle \Psi_0 | H_e | \Psi_0 \rangle$ should use some wavefunction Ψ_0 which, of course, is the function of nuclear positions $\{R\}$. Therefore, in classical mechanics, the forces on the nuclei can be obtained from the derivative of the Lagrangian with respect to nuclear positions. This means that the functional derivative with respect to the orbitals, which can be considered as classical fields, can give forces for orbitals, using an appropriate Lagrangian. It should be noted that some restrictions for the orbitals should be introduced, for example, the conditions of orthonormalization.

For the molecular dynamics of Car-Parrinello the following class of Lagrangians is introduced:

$$\mathcal{L}_{CP} = \underbrace{\sum_I \frac{1}{2} M_I \dot{\mathbf{R}}_I^2 + \sum_i \frac{1}{2} \mu_i \langle \dot{\psi}_i | \dot{\psi}_i \rangle}_{\text{kinetic energy}} - \underbrace{\langle \Psi_0 | \mathcal{H}_e | \Psi_0 \rangle}_{\text{potential energy}} + \underbrace{\text{constraints}}_{\text{orthonormality}} \quad (13)$$

The relevant Newtonian equations of motion derived from the corresponding Euler-Lagrange equations

$$\frac{d}{dt} \frac{\partial \mathcal{L}}{\partial \dot{\mathbf{R}}_I} = \frac{\partial \mathcal{L}}{\partial \mathbf{R}_I} \quad (14)$$

$$\frac{d}{dt} \frac{\delta \mathcal{L}}{\delta \dot{\psi}_i^*} = \frac{\delta \mathcal{L}}{\delta \psi_i^*} \quad (15)$$

appear as in classical mechanics, but for the nuclear positions and for the orbitals holonomic constraints should be applied $|\psi_i\rangle^* = \langle \psi_i|$. Using the Lagrange equations, the Car-Parrinello equations can be written as:

$$M_I \ddot{\mathbf{R}}_I(t) = -\frac{\partial}{\partial \mathbf{R}_I} \langle \Psi_0 | \mathcal{H}_e | \Psi_0 \rangle + \frac{\partial}{\partial \mathbf{R}_I} \{constraints\} \quad (16)$$

$$\mu_i \ddot{\psi}_i(t) = -\frac{\delta}{\delta \psi_i^*} \langle \Psi_0 | \mathcal{H}_e | \Psi_0 \rangle + \frac{\delta}{\delta \psi_i^*} \{constraints\} \quad (17)$$

where μ_i ($= \mu$) are "fictitious masses" assigned to the orbital degrees of freedom; one should note that these restrictions on the total wave function would lead to the limitation of force in the equations of motion. Note also, that these restrictions depend on the nuclear positions:

$$constraints = constraints(\{\psi_i\}, \{RI\}) \quad (18)$$

These relationships should be taken into account properly in deriving the Car-Parrinello equations following from the equation (13) and using formulas. (14) - (15).

According to the equations, the nuclei evolve in time at instantaneous physical temperature $\sum_i M R_i^2$, while the "fictitious temperature" $\sum_i \mu_i \langle \dot{\psi}_i | \dot{\psi}_i \rangle$ describes the changes for electronic degrees of freedom. Therefore, the "low temperature" of the electrons means that the electronic subsystem is close to the ground state (or close to the BO surface). Therefore, an important task is to separate in practice nuclear and electronic motion so that the fast electronic subsystem stays 'cold' during the simulation time, but at the same time, the condition of adiabaticity for the nuclear motion should be satisfied. At the same time, the nuclei nevertheless remain at a much higher temperature than electrons. This is possible if the power spectra of electrons and nuclei do not have a significant overlap in the frequency domain, so that the transfer of energy from "hot cores" in the "cold electrons" becomes practically impossible in the relevant time. In the next chapter we will consider how to control adiabaticity [2].

1.2.2.3 How to Control Adiabaticity?

Here, we will consider the adiabatic separation of electronic and nuclear degrees of freedom for Car-Parrinello *MD*. The second important question is how to provide this separation. A simple harmonic analysis of the frequency spectrum of the orbital for classical fields close to the minimum of energy gives the ground state

$$\omega_{ij} = \left(\frac{2(\epsilon_i - \epsilon_j)}{\mu} \right)^{1/2} \quad (19)$$

where ϵ_i and ϵ_j denote the eigenvalues of occupied and unoccupied orbitals, correspondingly. This holds true for the lowest frequency ω_e^{\min} and a convenient analytical evaluation of the lowest possible frequency of the electronic indicates that this frequency is a function of the square root of the electronic energy difference E_{gap} between lowest unoccupied and highest occupied orbitals

$$\omega_e^{\min} \propto \left(\frac{E_{\text{gap}}}{\mu} \right)^{1/2} \quad (20)$$

On the other hand, we can control the minimum frequency by varying the parameter of fictitious mass μ .

In order to provide the adiabatic separation, the frequency difference $\omega_e^{\min} - \omega_e^{\max}$ should be large enough. However, the phonon frequencies for the system ω_e^{\max} and E_{gap} should be determined by the properties of the system.

So we can conclude, that the only parameter in our hands to control adiabatic separation is the fictitious mass, which is called "parameter of adiabaticity ". However, the decrease μ shifts the electronic spectrum upwards on the frequency scale, and also extends across the full spectrum of frequencies in accordance with the equation (19). This leads to an increase in the maximum frequency in accordance with the equation (21)

$$\omega_e^{\max} \propto \left(\frac{E_{\text{cut}}}{\mu} \right)^{1/2} \quad (21)$$

where E_{cut} is the maximum kinetic energy if the plane waves are used. However, according to the equation (22) the maximal timestep is directly proportional to fictitious mass and it is inversely proportional to the highest frequency in the system:

$$\Delta t^{\max} \propto \left(\frac{\mu}{E_{\text{cut}}} \right)^{1/2} \quad (22)$$

As a consequence, it is necessary to find a compromise for the value of the fictitious mass, typical values for large gap of $\mu = 500\text{-}1500 m_e$ together with a step of about 5-10 atomic units (0.12-0.24 fs). A recently developed algorithm optimizes μ during the simulation for a fixed criterion of accuracy. [2].

1.2.2.4 The Quantum Chemistry Viewpoint

Here, we consider the molecular dynamics of Car–Parrinello from the standpoint of quantum chemistry. Let us write the Lagrangian of *CP* in the following form:

$$\begin{aligned} \mathcal{L}_{CP} = & \sum_I \frac{1}{2} M_I \dot{\mathbf{R}}_I^2 + \sum_i \frac{1}{2} \mu_i \langle \dot{\psi}_i | \dot{\psi}_i \rangle \\ & - \langle \Psi_0 | \mathcal{H}_e^{\text{HF}} | \Psi_0 \rangle + \sum_{i,j} \Lambda_{ij} (\langle \psi_i | \psi_j \rangle - \delta_{ij}) \end{aligned} \quad (23)$$

The resulting equations of motion

$$M_I \ddot{\mathbf{R}}_I(t) = -\nabla_I \langle \Psi_0 | \mathcal{H}_e^{\text{HF}} | \Psi_0 \rangle \quad (24)$$

$$\mu_i \ddot{\psi}_i(t) = -\mathcal{H}_e^{\text{HF}} \psi_i + \sum_j \Lambda_{ij} \psi_j \quad (25)$$

are very close to the equations which were obtained for the Born-Oppenheimer molecular dynamics equations. (12), but we have got certain features:

1. There is no need to minimize the total electronic energy expression involving an additional fictitious kinetic energy

2. The additional fictitious kinetic energy associated with the orbital degrees of freedom is due to the use of *CP* Lagrangian.

This means that both sets of equations become identical if the second derivative of the term $|\mu_i \psi_i(t)|$ is small at any given time t compared with the corresponding physical forces on the right side of the equations (24) - (25). This term is equal to zero if the energy of the electronic system will be close to the minimum $\langle \Psi_0 | H_e^{HF} | \Psi_0 \rangle$. In that case, the time derivatives of the orbitals $\{\psi_i\}$ can be considered as variations of Ψ_0 , and thus, it can be considered as the average value (H_e^{HF}) itself [2].

1.3 Electronic Structure Methods

In this chapter, density functional theory is presented only as a part of *ab initio* molecular dynamics. For simplicity, the formulae are presented for the spin-unpolarized or restricted special case. Density Functional Theory has been deeply investigated by D. Marx and Jurg Hutter in their work ‘Ab Initio Molecular Dynamic: Theory and implementation, John von Neumann Institute for Computing, 2000’ [2]. Below we use this text to describe Density Functional Theory, basis sets and pseudopotentials.

1.3.1 Density Functional Theory

Let us describe the density-functional theory. The total ground-state energy of the interacting system of electrons with classical nuclei fixed at positions $\{R_I\}$ can be obtained

$$\min_{\Psi_0} \{ \langle \Psi_0 | \mathcal{H}_e | \Psi_0 \rangle \} = \min_{\{\phi_i\}} E^{\text{KS}}[\{\phi_i\}] \quad (26)$$

as the minimum of the Kohn-Sham energy

$$E^{\text{KS}}[\{\phi_i\}] = T_s[\{\phi_i\}] + \int dr V_{\text{ext}}(\mathbf{r}) n(\mathbf{r}) + \frac{1}{2} \int dr V_{\text{H}}(\mathbf{r}) n(\mathbf{r}) + E_{\text{xc}}[n] \quad (27)$$

which can be described using a set of additional auxiliary functions. These functions should be orthonormal with respect to each other : $\langle \phi_i | \phi_j \rangle = \delta_{ij}$.

Therefore, the many body wavefunction is replaced by the set of orthonormal one-particle functions, Kohn-Sham orbitals $\{\phi_i\}$. It should be noted that this is a gross oversimplification. In that case the electronic one-body density

$$n(\mathbf{r}) = \sum_i^{\text{occ}} f_i |\phi_i(\mathbf{r})|^2 \quad (28)$$

should be obtained from a single Slater determinant constructed from the occupied orbitals, where f_i are the integers describing the occupation of the orbitals. The first term in the Kohn–Sham functional (see the equation (29)) describes the kinetic energy in the case of non-interacting system

$$T_s[\{\phi_i\}] = \sum_i^{\text{occ}} f_i \left\langle \phi_i \left| -\frac{1}{2}\nabla^2 \right| \phi_i \right\rangle \quad (29)$$

composed of the same number of electrons for the same external potential as in the case of fully interacting system. The second term describes the fixed external potential

$$V_{\text{ext}}(\mathbf{r}) = -\sum_I \frac{Z_I}{|\mathbf{R}_I - \mathbf{r}|} + \sum_{I < J} \frac{Z_I Z_J}{|\mathbf{R}_I - \mathbf{R}_J|} \quad (30)$$

in which the electrons move; this term includes the Coulomb interaction between electrons and nuclei, the second term of the equation (30) describes the interaction between the nuclei.

The third term describes the Hartree energy. Hartree energy is the classical electrostatic energy of two charges of clouds, which are derived from the electron density and can be obtained from the Hartree potential.

$$V_H(\mathbf{r}) = \int d\mathbf{r}' \frac{n(\mathbf{r}')}{|\mathbf{r} - \mathbf{r}'|} \quad (31)$$

which is defined by the electronic density via Poisson's equation

$$\nabla^2 V_H(\mathbf{r}) = -4\pi n(\mathbf{r}). \quad (32)$$

The last term in the Kohn-Sham functional is the exchange-correlation functional $E_{xc}[n]$. This term describes the most difficult contribution to the total electronic energy. Typically, the correlation and exchange effects are united; they are described by different types of analytic functions (see the chapter 1.3.7).

In order to obtain the minimum of the Kohn-Sham functional (equation (27)), it should be varied with respect to the density equation (28) or by using the orthonormality conditions of the orbitals. Thus, we can write the following Kohn-Sham equations

$$\left\{ -\frac{1}{2}\nabla^2 + V_{\text{ext}}(\mathbf{r}) + V_{\text{H}}(\mathbf{r}) + \frac{\delta E_{xc}[n]}{\delta n(\mathbf{r})} \right\} \phi_i(\mathbf{r}) = \sum_j \Lambda_{ij} \phi_j(\mathbf{r}) \quad (33)$$

$$\left\{ -\frac{1}{2}\nabla^2 + V^{\text{KS}}(\mathbf{r}) \right\} \phi_i(\mathbf{r}) = \sum_j \Lambda_{ij} \phi_j(\mathbf{r}) \quad (34)$$

$$H_e^{\text{KS}} \phi_i(\mathbf{r}) = \sum_j \Lambda_{ij} \phi_j(\mathbf{r}) \quad (35)$$

which describe the equation including the electronic one-particle Hamiltonian H_e^{KS} with a local potential V^{KS} . Note that the exchange and correlation effects are described, despite that the single-particle Hamiltonian has been used

$$\frac{\delta E_{xc}[n]}{\delta n(\mathbf{r})} = V_{xc}(\mathbf{r}) \quad (36)$$

Also, the canonical form of this equation can be obtained for this case

$$H_e^{\text{KS}} \phi_i = \epsilon_i \phi_i \quad (37)$$

of the Kohn-Sham equations, where $\{\epsilon_i\}$ are the eigenvalues.

For the case of the traditional static density functional theory, the system of equations must be solved self-consistently in order to obtain the density, the orbitals and the Kohn-Sham potential for the electronic ground state. The relevant equation for the total energy (see the equation 27) can be written as:

$$E^{\text{KS}} = \sum_i \epsilon_i - \frac{1}{2} \int d\mathbf{r} V_{\text{H}}(\mathbf{r}) n(\mathbf{r}) + E_{xc}[n] - \int d\mathbf{r} \frac{\delta E_{xc}[n]}{\delta n(\mathbf{r})} n(\mathbf{r}) \quad (38)$$

where the sum over ‘Kohn-Sham’ eigenvalues is a “band-structure energy”.

Equations (33) and (35) together with the equation (12) describe the case of Born-Oppenheimer molecular dynamics within Kohn-Sham density functional theory. The functional derivative of the Kohn-Sham functions with respect to the orbitals (so-called ‘Kohn-Sham force’) can be written as:

$$\frac{\delta E^{\text{KS}}}{\delta \phi_i^*} = f_i H_e^{\text{KS}} \phi_i \quad (39)$$

Therefore, equations (26) - (27) should be solved using the effective one-particle Hamiltonian in the Kohn-Sham formulation (see equations (35) - (37)). Crucial to any application of density functional theory is the approximation of the unknown exchange and correlation functional. Different types of functional for exchange and correlation energy are discussed in the chapter 1.3.7 [2].

1.3.2 How to solve Kohn-Sham equations?

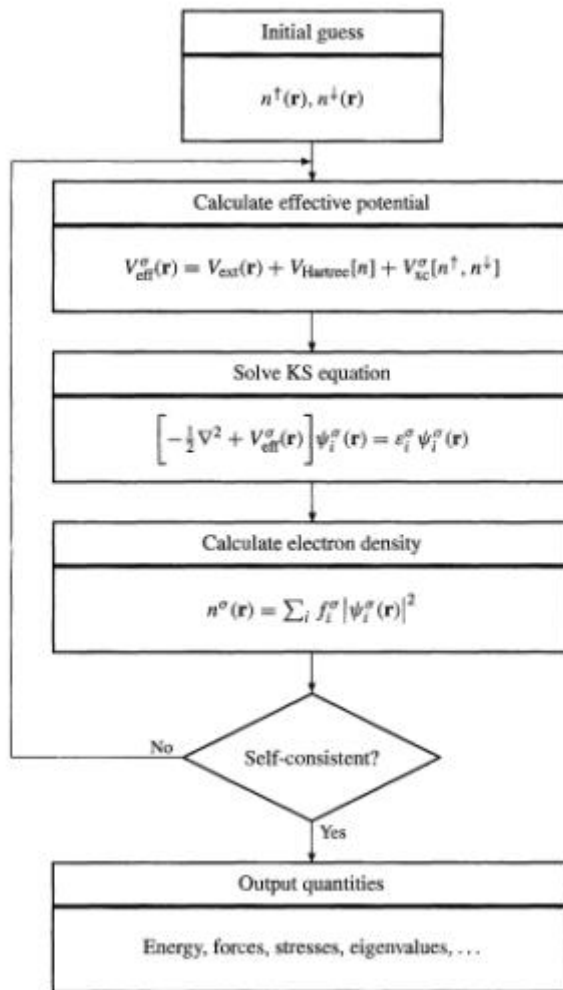


Figure 1. The self-consistent solution of Kohn-Sham equations, which have the form of one-particle Schrödinger equation.

A typical scheme for solving the Kohn-Sham equations is shown in figure 1. As a rule, the process of solution consists of the following steps:

1. At the first stage, the initial electron density must be set.
2. Then, the equations of Kohn-Sham are solved, which allow us to find an improved value for the electron density.
3. Next, the procedure is repeated until self-consistency criteria are achieved.
4. The values obtained in the solving of Kohn-Sham equations are used to calculate the observable characteristics of a system [1].

1.3.3 Hartree-Fock Theory

Hartree-Fock approximation is obtained by applying the variational principle in a limited space of wave functions. The ground state wave function is approximated by the Slater determinant $\Psi_0 = \det\{\psi_i\}$, which can be constructed from a set of single-particle orbitals. It should be noted that the wave function must be antisymmetric, in addition, the single-particle wave functions must be orthonormal to respect to each other $\langle \psi_i | \psi_j \rangle = \delta_{ij}$. It is easy to see, that the energy minimum in this case H_e :

$$\begin{aligned}
 E^{\text{HF}}[\{\psi_i\}] &= \sum_i \int d\mathbf{r} \psi_i^*(\mathbf{r}) \left[-\frac{1}{2}\nabla^2 + V_{\text{ext}}(\mathbf{r}) \right] \psi_i(\mathbf{r}) \\
 &+ \frac{1}{2} \sum_{ij} \int \int d\mathbf{r} d\mathbf{r}' \psi_i^*(\mathbf{r}) \psi_j^*(\mathbf{r}') \frac{1}{|\mathbf{r} - \mathbf{r}'|} \psi_i(\mathbf{r}) \psi_j(\mathbf{r}') \\
 &+ \frac{1}{2} \sum_{ij} \int \int d\mathbf{r} d\mathbf{r}' \psi_i^*(\mathbf{r}) \psi_j^*(\mathbf{r}') \frac{1}{|\mathbf{r} - \mathbf{r}'|} \psi_j(\mathbf{r}) \psi_i(\mathbf{r}')
 \end{aligned} \tag{40}$$

gives the lowest energy and the "best" wave function for the case of a single-determinant approximation, the external Coulomb potential V_{ext} has already been defined in the equation (30). Holding the restriction leads to

$$\left\{ -\frac{1}{2}\nabla^2 + V_{\text{ext}}(\mathbf{r}) + \sum_j \mathcal{J}_j(\mathbf{r}) - \sum_j \mathcal{K}_j(\mathbf{r}) \right\} \psi_i(\mathbf{r}) = \sum_j \Lambda_{ij} \psi_j(\mathbf{r}) \tag{41}$$

$$\left\{ -\frac{1}{2}\nabla^2 + V^{\text{HF}}(\mathbf{r}) \right\} \psi_i(\mathbf{r}) = \sum_j \Lambda_{ij} \psi_j(\mathbf{r}) \tag{42}$$

$$H_e^{\text{HF}} \psi_i(\mathbf{r}) = \sum_j \Lambda_{ij} \psi_j(\mathbf{r}) \tag{43}$$

which are similar equations for the Kohn-Sham equations which were obtained previously (see equations 33-35). We have got effective single-particle equations, which contain the Hartree-Fock operator H_e^{HF} . The canonical form for the case of the Kohn-Sham method

$$H_e^{\text{HF}} \psi_i = \epsilon_i \psi_i \tag{44}$$

is obtained as well as in the case of Kohn-Sham equations (see the equation 37). The Coulomb operator is

$$\mathcal{J}_j(\mathbf{r}) \psi_i(\mathbf{r}) = \left[\int d\mathbf{r}' \psi_j^*(\mathbf{r}') \frac{1}{|\mathbf{r} - \mathbf{r}'|} \psi_j(\mathbf{r}') \right] \psi_i(\mathbf{r}) \quad (45)$$

and the exchange operator can be written as

$$\mathcal{K}_j(\mathbf{r}) \psi_i(\mathbf{r}) = \left[\int d\mathbf{r}' \psi_j^*(\mathbf{r}') \frac{1}{|\mathbf{r} - \mathbf{r}'|} \psi_i(\mathbf{r}') \right] \psi_j(\mathbf{r}) \quad (46)$$

The force acting on the orbitals (or the functional derivative) has the same form as in the case of a Kohn-Sham method (see the equation 39)

$$\frac{\delta E^{\text{HF}}}{\delta \psi_i^*} = H_e^{\text{HF}} \psi_i \quad (47)$$

It can be concluded, that the various *ab initio* molecular dynamics schemes based on Hartree-Fock theory are defined for Born-Oppenheimer molecular dynamics (see equation 12) and for Car-Parrinello molecular dynamics (see equations (26) and (27)) [2].

1.3.4 Comparison between Hartree-Fock and Kohn-Sham methods

As seen from the preceding discussion, the exact solution for the many-electron problem it is necessary to find the correlation and exchange energy, which includes, as its name implies, the energy of electron correlation. In other words, the density functional theory, in spite of one-particle representation of the wave function takes into account the correlation energy, and, in principle, can do it accurately. The only problem is that the form of exchange-correlation functional is unknown, and therefore it is necessary to establish an approximate formula for it. Before describing the existing approaches for exchange-correlation energy, give a brief comparative description of the Hartree-Fock theory and density functional theory. As noted above, both of which have very similar mathematical formalism, based on a variational principle, using an iterative procedure, and have approximately the same costs on the order of h^4 . At the same time, there are fundamental differences between methods of Hartree-Fock and *DFT*, which can be formulated as the following questions:

- A. Is it possible in principle to obtain an exact solution? If one knew the exact value for E_{XC} , *DFT* would give the possibility to calculate the exact value of the total energy, including an electron correlation. And it is using the same computational cost, as well as to calculate the uncorrelated Hartree-Fock energy! However, it is possible that the exact $E_{XC}[\rho]$ functional can be so complex that the computational cost will be comparable to those of the exact solution of the Schrödinger equation with traditional methods of wave mechanics. Hartree-Fock method, in principle, cannot give an exact solution of the wave equation, and for the Hartree-Fock limit is only reachable for *DFT* methods.
- B. What about the accuracy of the solution? Hartree-Fock one-electron equations are solved rigorously, because iterative procedure, in principle, allows to reach any reasonable threshold for small convergence of the solution. Although the *DFT* approximations also use self-consistent procedure, the matrix elements for the Kohn-Sham approximation, are not calculated as strictly, because one does not know the exact form of correlation-exchange functional. Since, the exact form of $E_{XC}[\rho]$ is still unknown, we can ask the question: what computational costs are needed to obtain the result of required accuracy? That is why *DFT* method looks especially attractive [1].

1.3.5 Basis Sets

1.3.5.1 Gaussians and Slater Functions

In practice, the solution of equation (44) must represent a molecular orbital ψ_i (wave function of the system) as a combination of atomic orbitals (*AO*) (atomic wave functions in the system), which in turn can be represented as a linear combination of a finite number of basis states. The choice of the basis of atomic functions is an important task, as it defines how accurately the expansion (48) approximates the molecular orbital.

This series should converge rapidly, i.e., a small number of basis functions should describe the total orbital with the required accuracy. There are three main criteria for selection of basic functions:

1. The basis functions should give a good approximation to the correct wave function (for example, near the nuclei and at large distances from them).

2. The basis functions should allow an analytical calculation of the required integrals.
3. The total number of basis functions should not be very large.

Let us consider a typical equation for basis functions

$$\psi_i(\mathbf{r}) = \sum_{\nu} c_{i\nu} f_{\nu}(\mathbf{r}; \{\mathbf{R}_I\}) \quad . \quad (48)$$

Obviously, this equation describes a linear combination of basis functions. The selected functions f_{ν} should have a well-known properties; $c_{i\nu}$ are the expansion coefficients.

Currently, widely used the next set of basis functions:

- Slater-type basis functions (*STOs*)

$$f_{\mathbf{m}}^{\text{S}}(\mathbf{r}) = N_{\mathbf{m}}^{\text{S}} r_x^{m_x} r_y^{m_y} r_z^{m_z} \exp[-\zeta_{\mathbf{m}}|\mathbf{r}|] \quad (49)$$

- Gaussian-type basis functions (*GTOs*)

$$f_{\mathbf{m}}^{\text{G}}(\mathbf{r}) = N_{\mathbf{m}}^{\text{G}} r_x^{m_x} r_y^{m_y} r_z^{m_z} \exp[-\alpha_{\mathbf{m}}r^2] \quad (50)$$

where $N_{\mathbf{m}}$, $\zeta_{\mathbf{m}}$ and $\alpha_{\mathbf{m}}$ are constants that are typically kept fixed during an electronic structure calculation so that only the orbital expansion coefficients $c_{i\nu}$ should be optimized.

- Plane waves. This type of basic set is described in the following chapter [2].

1.3.5.2 Plane Waves

Plane waves basis set is widely used to describe atomic orbitals for periodic systems. The main advantages of plane waves are the properties of completeness and orthonormality. Expansion in plane waves is usually described with good accuracy, the calculation of the electronic structure of periodic crystal structure. Also, this expansion can be successfully applied to calculate finite and disordered systems, such as atomic clusters or structures with defects. From a mathematical point of view, only the plane waves form a complete basis set, i.e. by increasing the number of basis functions accuracy of solution for Fock equations, also will increase.

Plane waves are defined as:

$$f_G^{\text{PW}}(\mathbf{r}) = N \exp[i\mathbf{G}\mathbf{r}] \quad , \quad (51)$$

where the normalization is simply given by $N = 1/\sqrt{\Omega}$; Ω is the volume of the periodic (super-) cell.

It is important to note that plane waves do not depend on the position of the nuclei $\{R_i\}$. This means that plane waves are delocalized in space and do not belong to certain atoms which means that they can be viewed as ultimately "balanced basis set" in the language of quantum chemistry [2].

1.3.6. Pseudopotentials

As described above, one of the widely used basis set is a set of plane waves. Its main advantages are the properties of completeness and orthonormality. Unfortunately, its direct application to describe the wave functions of electrons in molecular and crystal structures is severely limited by the fact that the electron wave function near the nuclei of atoms oscillates rapidly (see the figure 2) and its expansion into plane waves require a huge number of terms in the expansion (estimates for the Al atom gives the number of terms in the expansion functions $N \sim 10^6$).

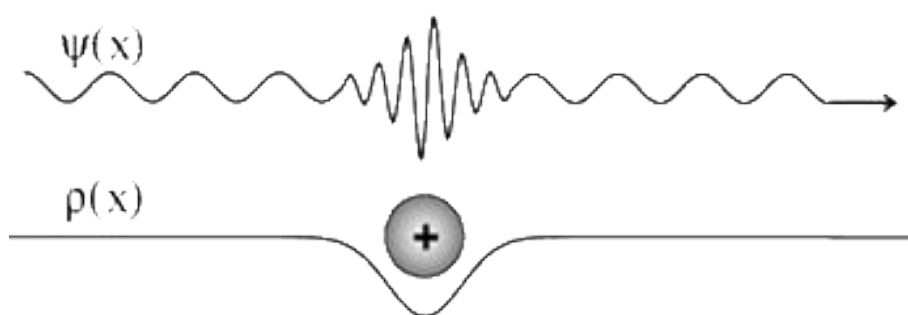


Figure 2. Electron wave function undergoes oscillations near the nucleus of an atom.

The essence of the pseudopotential theory consists precisely to reduce the degree of valence oscillations of the calculated wave functions near the nucleus of an atom. In this case only the valence electrons are calculated, because it is known that most of the physical properties of a physical system depend precisely on the behavior of valence electrons. The 'core' electrons

are the same, i.e. it is assumed that the behavior of the wave functions of core electrons remains unchanged under the influence of an external chemical environment of the atom. This procedure is equivalent to replacing the strong electron-ion potential by a weaker pseudopotential, which defines all the explicit properties of the valence electrons, including relativistic effects.

First of all, the pseudopotential should be norm-conserving. Norm-conserving pseudopotentials have to be angular momentum dependent. In their most general form they are semi-local

$$V^{PP}(\mathbf{r}, \mathbf{r}') = \sum_{lm} Y_{lm}(\mathbf{r}) V_l(\mathbf{r}) \delta_{\mathbf{r}, \mathbf{r}'} Y_{lm}(\mathbf{r}') \quad (52)$$

where Y_{lm} are spherical harmonics [2]. The minimal requirements have been proposed for the development of pseudopotentials. Since then, many different methods have been proposed for the construction of the pseudopotential. Originally pseudopotential is generated in a semi-local form, and most applications use fully separable form. Pseudopotentials can be converted into a separable form of the atomic wave functions.

There are four universally accepted criteria for selecting the optimal pseudopotential:

- Pseudowave function should not contain nodes. This is necessary to obtain a smooth pseudowave function.
- Pseudowave function must be continuous and twice differentiable.
- The charges, which are concentrated within a sphere of radius r_c , for the wave functions from the both sides of r_c must be the same.
- The eigenvalues of the two wave functions must also be equal from the both sides of r_c [3].

1.3.7 Exchange and correlation in DFT

In this chapter we will discuss the form of exchange (E_x) and correlation energy (E_c). It is possible to prove that the exchange-correlation potential is a unique functional strict for all systems. However, the specific form of this potential is not established yet. Various *DFT* methods differ only in the choice forms of $E_{XC}[p]$ functional and the presence of different sets

of adjustable parameters. The usual approach is to divide E_{xc} on the exchange (E_x) and correlational (E_c) potentials, although the severity of this separation is not well established [3]:

$$E_{xc}[\rho] = E_x[\rho] + E_c[\rho] = \int \rho(r)\varepsilon_x(\rho(r))dr + \int \rho(r)\varepsilon_c(\rho(r))dr. \quad (53)$$

1.3.7.1. The Local Density Approximation (LDA)

Several types of functionals have been suggested for E_x and E_c . The local density approximation (or local spin density approximation (*LSDA*) in a more general case) has been used widely. This approximation assumes that the local electron density is a homogeneous electron gas, which means that the electron density changes very slowly.

The exchange energy density is given by the equation of Dirac:

$$\varepsilon_x^{LSDA}[\rho] = -2^{1/3} C_x (\rho_\alpha^{1/3} + \rho_\beta^{1/3}), \quad (54)$$

where:

$$C_x = \frac{3}{4} \left(\frac{3}{\pi} \right)^{1/3}. \quad (55)$$

ρ_α and ρ_β are spin densities, i.e. the electronic densities, for individual electronic systems produced separately by electrons from systems α and β .

The same equation can be written in terms of the total density and spin polarization ζ :

$$\varepsilon_x^{LSDA}[\rho] = -2^{1/3} C_x \rho^{1/3} [(1+\zeta)^{4/3} + (1-\zeta)^{4/3}], \quad \zeta = \frac{\rho_\alpha - \rho_\beta}{\rho_\alpha + \rho_\beta}. \quad (56)$$

Correlation energy density of a homogeneous electron gas is calculated by analytical interpolation formula of Vosko, Wilk, Nusair, which contains unpolarized ($\zeta = 0$) and polarized ($\zeta = 1$) components:

$$\begin{aligned} \varepsilon_c^{VWN}(r_s, \zeta) = & \varepsilon_c(r_s, 0) + \varepsilon_a(r_s) \frac{f(\zeta)}{f''(0)} (1 - \zeta^4) + \\ & + [\varepsilon_c(r_s, 1) - \varepsilon_c(r_s, 0)] f(\zeta) \zeta^4, \end{aligned} \quad (57)$$

where:

$$r_S = \left(\frac{3}{4\pi\rho} \right)^{1/3} \quad (58)$$

$$f(\zeta) = \frac{(1+\zeta)^{4/3} + (1-\zeta)^{4/3} - 2}{2(2^{1/3} - 1)} \quad (59)$$

Functionals ε_c and ε_a are defined by equations containing a number of adjustable parameters. According to the formulas proposed by Perdew and Wang:

$$\varepsilon_{c/a}^{PW91} = -2a\rho(1 + \alpha x^2) \ln \left(1 + \frac{1}{2a(\beta_1 x + \beta_2 x^2 + \beta_3 x^3 + \beta_4 x^4)} \right) \quad (60)$$

where:

$$x = r_S^{1/2}; a, \alpha, \beta_1, \beta_2, \beta_3, \beta_4 \quad (61)$$

are some constants.

The accuracy of methods based on *LSDA* approximation is comparable with the accuracy of Hartree-Fock methods [1].

1.3.7.2 The generalized gradient approximation (GGA)

More accurate results are obtained by using the generalized gradient approximation method connecting E_X and E_C not only with the electronic density but also with its first $\nabla\rho$ and second ($\nabla^2\rho$) derivatives. Several functional dependencies were suggested in the form of amendments to the *LSDA* functionals.

For example, the exchange correction of Becke:

$$\varepsilon_X^{B88} = \varepsilon_X^{LDA} + \Delta\varepsilon_X^{B88}, \quad \Delta\varepsilon_X^{B88} = -\beta\rho^{1/3} \frac{x^2}{1 + 6\beta x \sinh^{-1} x}, \quad x = \frac{|\nabla\rho|}{\rho^{4/3}} \quad (62)$$

This parameter β is obtained from the known data for the atoms. Exchange and correlation functionals defined by Perdew and Wang (but with corrective terms) are also widely used. For example, the formula for the exchange energy density has the form:

$$\varepsilon_X^{PW91} = \varepsilon_X^{LDA} \left(\frac{1 + xa_1 \sinh^{-1}(xa_2) + (a_3 + a_4 \exp(-bx^2))x^2}{1 + xa_1 \sinh^{-1}(xa_2) + a_5x^2} \right), \quad (63)$$

where a 1-5 and b are fitted constants, and x has the same sense as in the equation for *LDA*. The correlation functional has the form:

$$\varepsilon_C^{PW91} = \varepsilon_C^{LDA} + \Delta\varepsilon_C^{PW91}. \quad (64)$$

Analytical equation for the correction to the correlation functional $PW91 \Delta\varepsilon_C^{PW91}$ can be found in the literature. Also, there are some functionals with gradient correction (not amendments!). For example, one of the most popular correlation functionals proposed by Lee, Yang and Parr (*LYP* functional) has the next form:

$$\varepsilon_C^{LYP} = -4a \frac{\rho_\alpha \rho_\beta}{\rho^2 (1 + d\rho^{-1/3})} - ab\omega \left\{ \begin{aligned} & \frac{\rho_\alpha \rho_\beta}{18} X + \frac{2}{3} \rho^2 (|\nabla \rho_\alpha|^2 + |\nabla \rho_\beta|^2 - \\ & - |\nabla \rho|^2) - (\rho_\alpha^2 |\nabla \rho_\beta|^2 + \rho_\beta^2 |\nabla \rho_\alpha|^2) \end{aligned} \right\}$$

$$X = 144(2^{2/3})C_F(\rho_\alpha^{8/3} + \rho_\beta^{8/3}) + (47 - 7\delta)|\nabla \rho|^2 - (45 - \delta) \times$$

$$\times (|\nabla \rho_\alpha|^2 + |\nabla \rho_\beta|^2) + 2\rho^{-1}(11 - \delta)(\rho_\alpha |\nabla \rho_\alpha|^2 + \rho_\beta |\nabla \rho_\beta|^2),$$

$$\omega = \frac{\exp(-c\rho^{-1/3})}{(1 + d\rho^{-1/3})\rho^{14/3}}, \quad \delta = c\rho^{1/3} + \frac{d\rho^{-1/3}}{1 + d\rho^{-1/3}}, \quad (65)$$

where:

$$C_F = \frac{3}{10}(3\pi^2)^{2/3} \quad (66)$$

where a , b , c and d are parameters determined by fitting to experimental data for the helium atom.

Adding members to the nonlocal *LSDA* functional calculations significantly improves the quality of structural parameters of molecules as well as energy characteristics [1].

1.3.7.3. Hybrid HF-KS approaches

Nowadays, the so-called hybrid methods have been developed, in which correction for E_X is taken into account, calculated as the exchange energy in the Hartree-Fock (of course, only Kohn-Sham orbitals are used).

For example, the Becke functional which includes 3 parameters (*B3*) is an example of a hybrid functional:

$$E_{XC}^{B3} = (1-a)E_X^{LSDA} + a \cdot E_X^{HF} + b \cdot \Delta E_X^{B88} + E_C^{VWN} + c \cdot \Delta E_C^{GGA} \quad (67)$$

where, the Hartree-Fock exchange energy E_X^{HF} with the contribution a is a part of expression for the exchange functional. Equations for the second, third and fourth terms in the sum were discussed above. The last term in the sum ΔE_C^{GGA} is a correction of the gradient correlation functional.

Various implementations of the hybrid DFT method can be obtained using different correction types. Thus, the use of amendments of Purdue and Wang (GGA = PW91) gives a popular method B3PW91. Currently, in the most widespread *DFT* method ΔE_C^{GGA} is used instead of correlation functional of Lee, Yang and Parr (*LYP*), leading to the well-known acronym *B3LYP*. Since, the functional *LYP* contains local and nonlocal terms, and then the correlation-exchange functional *B3LYP* method, in fact, has the form:

$$E_{XC}^{B3LYP} = (1-a)E_X^{LSDA} + a \cdot E_X^{HF} + b \cdot \Delta E_X^{B88} + (1-c)E_C^{VWN} + c \cdot E_C^{LYP}, \quad (68)$$

a , b and c are constants which were chosen Becke from reliable experimental data for a representative set of relatively simple chemical compounds (the so-called *G1*-set).

Other examples of hybrid functional: *MPW1PW91* is one-parameter hybrid functional with the modified exchange functional of Perdew and Wang and with correlation functional *PW91*. This *DFT* method is used to calculate the chemical shifts and hyperfine coupling constants of *NMR* spectra with an excellent degree of accuracy; *G961LYP* - is one-parameter hybrid functional with the exchange functional of Gill *G96* and with the *LYP* correlation functional,

etc. Wide practical use of hybrid *DFT* methods connected with the unique combination of low-cost approach and high degree of accuracy of simulation results, is comparable (and sometimes superior!) with an accuracy of such complex methods as *MP2*, *MP4*, *QCISD*, and *CCSD* [1].

1.4.1. Reverse Monte Carlo Modelling

An excellent review for the *RMC* method was written by R.L. Mc Greevy. (R.L. Mc Greevy, ‘Reverse Monte Carlo. Topical review. J.Phys.:Condens. Matter 13(2001)’) [4]. This work has been used to explain the basic *RMC* algorithm, the main constraints and some common misconceptions of *RMC* method.

Reverse Monte Carlo (*RMC*) modelling is the main method of structural modeling. It based on experimental data. In *RMC* modelling, the starting point is a set of experimental data, and atomic configurations are produced in accordance with the procedure that is specifically designed to give better agreement with experimental data. *RMC* modeling can be applied to many different types of data simultaneously, if desired. Powder and single-crystal neutron diffraction, X-ray diffraction and electron diffraction, extended x-ray absorption fine structure and nuclear magnetic is used to provide data. *RMC* modeling can be used to various types of materials: liquids, glasses, polymers, crystals and etc [4].

1.4.2. The basic RMC algorithm

As a general rule, for *RMC* simulation the standard Metropolis Monte Carlo (*MMC*) method is used. The main goal is to produce a structural model (i.e., an ensemble of atoms, usually referred to as configuration), which agrees with one or more sets of experimental data within their errors, and taking into account the many constraints. Errors are purely statistical and have a normal distribution. Next, we will describe the typical *RMC* algorithm.

1. The starting point of *MC* is an initial configuration of atoms. *N* atoms are placed in a cell with periodic boundary conditions. Coordinates of atoms can be selected randomly or can correspond to a crystal atomic structure.
2. Calculate the atomic scattering function based on atomic coordinates.
3. After that, we need to move atoms randomly at some distance away from its original position.
4. If the distance between the displaced and any other atom smaller than a certain minimum distance, then this movement is canceled, go to step 3, otherwise go to step 5.
5. Now we need to calculate new functions (for example, the interference function, the pair correlation function) to compare with experimental data.
6. Calculate the difference between the measured calculated function, $F^E(Q)$, and that calculated from the configuration, $F^{Co}(Q)$:

$$\chi_o^2 = \sum_{i=1}^m (F^{Co}(Q_i) - F^E(Q_i))^2 / \sigma^2(Q_i) \quad (69)$$

where the sum is over the *m* experimental points and σ nominally represents the experimental error.

7. If $\chi_n < \chi_o$, then the move is accepted, i.e. the ‘new’ configuration becomes the ‘old’ configuration. If $\chi_n > \chi_o$ it is accepted with probability $\exp(-(\chi_n^2 - \chi_o^2)/2)$. Otherwise it is rejected.
8. Go to step 3.

During the simulation χ^2 will be reduced by the large number of atomic movements. The result of modeling is three-dimensional structure which agrees with experimental data.

There are several features of the Monte Carlo method which make it more successful in determining the atomic structure of materials in comparison with earlier attempts to use this method.

- First of all, the periodic boundary conditions are used to avoid finite-size effects.
- Secondly, some of the atomic movements associated with an increase in the χ^2 are accepted because the final simulation result does not depend on the initial configuration.
- In addition, the atomic potential is not used. The lack of the potential has the disadvantage that *MC* models have not the thermodynamic consistency [4].

1.4.3. Constraints

One of the general features of the *RMC* method is the use of constraints. The most important are the number of density and the use of cut-offs. Constraints are an important part of the main algorithm for *RMC*, and the initial factor in determining the structure for any system, so it makes sense to include them from the beginning. Without these constraints, *RMC* modeling will be able produce any set of data, as a rule with big mistakes, if the number of data points was less than the number of variables in the model. However, due to the restrictions the atomic coordinates are free variables, instead they are very limited.

Choices of cut-offs are not always evident and can be important if the available data are insufficient. So it must be at least one data set, and the shortest cut-off can always be estimated from the direct determination of the radial distribution function. Without other information, it should also be used as a cut-off distance for all atomic pairs. If several sets of data are available, it may be possible to estimate the cut-offs a few pairs of atoms. Most often, this can also be done using other evaluation information, such as atomic or ionic radii and the results for the corresponding systems.

The next most frequently used restrictions are the atomic coordinates. In a sense, these act to imitate covalent bonds and, therefore, be regarded as a form of many-body potential. The average atomic coordination can also be limited. One can also limit the coordination of individual atoms.

In principle, any restrictions can be applied for any system. For example, three-atom constraints; bond angles restrictions can also be used [4].

1.5 Classical methods of computer modelling

1.5.1 Classical Monte Carlo method

Monte Carlo (*MC*) method is a method which allows generating an infinite number of configurations for an available material. Implementation of Metropolis Monte Carlo method, which is common use in computational physics, requires the algorithm to generate a new configuration by modifying the previous configuration.

The main algorithm for Monte Carlo methods is presented below:

1. The starting point of *MC* is an initial configuration of atoms. N atoms are placed in a cell with periodic boundary conditions. Coordinates of atoms can be selected randomly or can correspond to a crystal atomic structure.
2. Calculate energy using an inter-atomic potential.
3. Calculate difference between initial and new configurations.
4. If the energy change is negative, leading to a lowering of the energy, the change is automatically accepted. But, if the energy change is positive, the new configuration is accepted with probability. $\exp(-\Delta E/k_B T)$
5. Move to step 1.

This procedure is repeated for a large number of steps leading to the evolution of an ensemble of atomic particles in time. This approach ensures that the sampling procedure is consistent with thermodynamics; for example, states with any energy E occur with the relative probability $\exp(E/k_B T)$.

The complete set of configurations, including duplicated configurations, can be analyzed to calculate averaged quantities which have the correct thermodynamic weighting automatically ensured. For example, it is possible to calculate the average energy as a function of temperature. Of course, as a rule, classical potential is used to estimate the energy of a system. [5].

1.5.2 Classical molecular dynamics method

Molecular dynamics is a classical method for time evolution of the system at a particular temperature. Molecular dynamic modeling consists of the numerical solution classical equation of motion, which for a simple atomic system may be written:

$$m_i \ddot{\mathbf{r}}_i = \mathbf{f}_i \quad \mathbf{f}_i = -\frac{\partial}{\partial \mathbf{r}_i} \mathcal{U} \quad (70)$$

For this purpose, it is necessary to calculate the forces, acting on atoms. Therefore, the potential should be chosen for our specific task.

For many ionic materials the predominant short-range potential used is the Buckingham potential, which consist of a repulsive exponential and an attractive dispersion term between pairs of atoms. For more general systems, such as molecular organics, semiconductors, metals a wider range of functional forms is required. In the most commonly used inter-atomic potentials cut-off is controlled by the dispersion term $-C/r^6$.

Molecular-dynamics experiment consists of four steps that are listed below:

1. **Initialization:** The conditions for simulation should be selected, including the coordinates of the atoms, their velocity and temperature.
2. **Equilibrium:** system should reach the equilibrium state. As soon as the equilibrium is reached, we can measure the thermodynamic characteristics of the system (for example, temperature and pressure). The equilibrium state characterizes the correct ratio between kinetic and potential energies and the Maxwell-Boltzmann distribution of velocities at a certain temperature. During this stage, the velocities scale to maintain the proper temperature. The time required to reach steady state depends on the nature and size of the system.
3. **Production:** At this stage, the system evolves without temperature scaling, depending on the chosen ensemble. The length of this phase depends on the purpose of modeling. For example, if the purpose of modeling is studying the diffusion phenomena and change of phase, then the simulation must be a long. But, if the goal is to study the vibrational properties of the system, then a short experiment in a few picoseconds would be sufficient.

4. **Analysis:** The results of modeling are the Cartesian coordinates and velocities of individual atoms and various characteristics of the system (temperature, pressure). This information is analyzed to calculate the desired characteristics.

The obvious advantage of Molecular Dynamic over Monte Carlo is that it gives a route to dynamical properties of system: transport coefficients, time-depend responses to perturbation, diffusion coefficients and vibration spectra. The molecular dynamics method is quite simple. However, software for this method requires further efforts related to the numerical methods in applied mathematics [6].

2. Experiment

2.1 Calculation software

We used the cp2k code [7] as the main software to perform "first-principles" molecular dynamic simulations. For comparison with physical experiments we used the synchrotron radiation data from the Japanese research group at Spring-8. As a rule, to create an initial configuration, we used the Reverse Monte Carlo method [8] (fitting data: x-ray diffraction). For "first-principles" calculations we used supercomputers in 'THE FINNISH IT CENTER FOR SCIENCE' [9] (CSC, Espoo).

2.2.1 Atomic structure of ZrO₂ (DFT MD simulation)

We performed *ab initio* simulation for 501 atoms in a cubic box with the length 18.98 Å. The temperature for this simulation was set to 3100 K (for the additional information about the simulation see the appendix № 2). As is well known, melting point for ZrO₂ is equal to 2750 K and the system size (501 atoms) is certainly adequate for simulating liquid material. The initial configuration was obtained after *RMC* refinement method (x-ray diffraction data; Spring-8, Japan). We used *BFGS* method to optimize the geometry for the structure. Thereafter, we performed *DFT* Molecular Dynamic simulation. The time for simulation was equal to 20 ps.

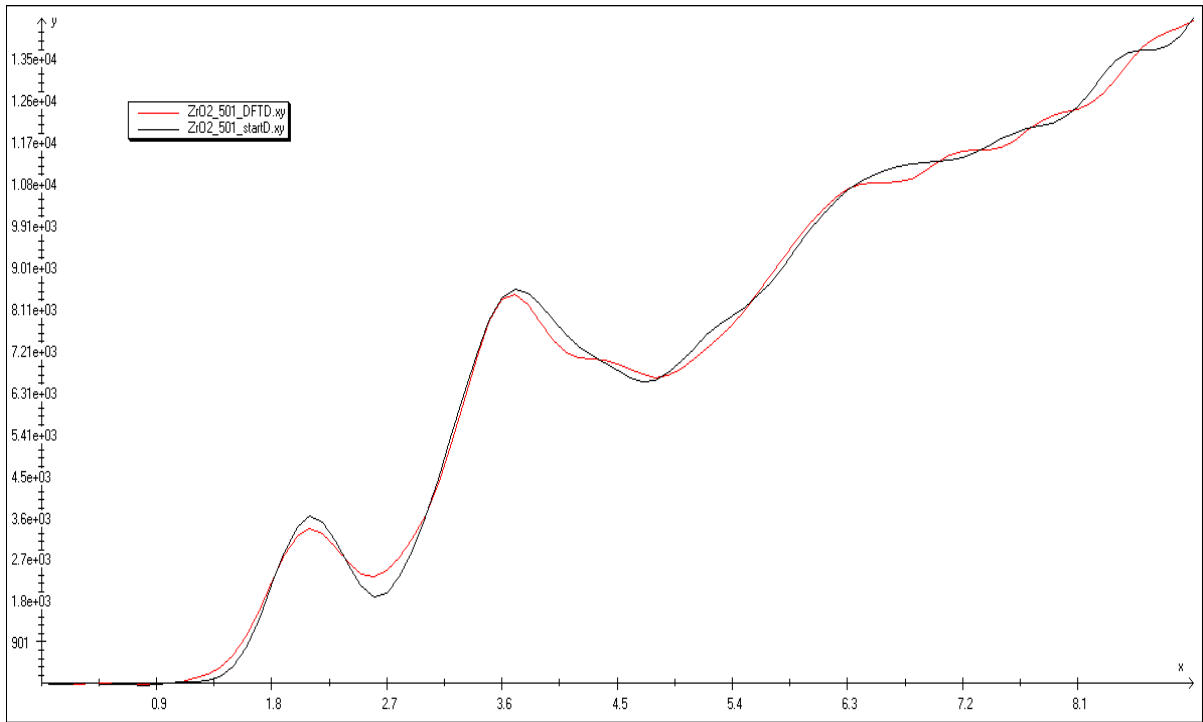


Figure 3. Total pair correlation functions. Red curve is the final configuration after *DFT* simulation. Black curve is the initial configuration for ZrO_2 .

Figure 3 shows the behavior of total correlation functions obtained after *DFT* (red curve) and *RMC* respectively. It is easy to see, that, the most probable distances for the structure are 2.12 (Zr-O distance) and 3.9 Å (O-O distance) (2 sharp peaks). The temperature for the simulation was equal to 3100 K, and during the simulation we obtained a liquid phase. Therefore, only the short-range order was obtained.

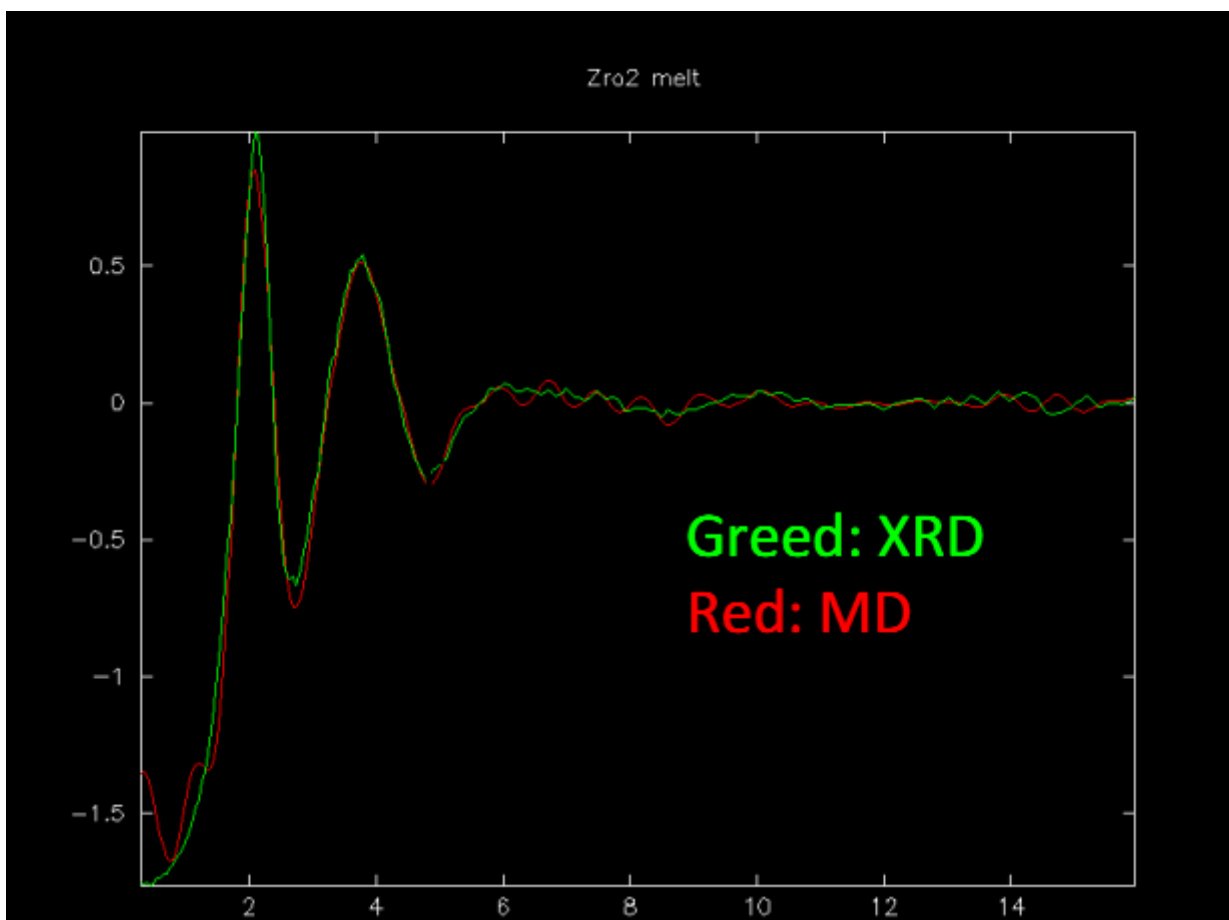


Figure 4. The total structure factor. Red curve is the final configuration after *DFT* simulation. Green curve is the initial configuration for ZrO_2 .

Figure 4 shows the behavior for total structure factors, which were obtained from the experiment (x-ray radiation, Spring-8, Tokyo, Japan) and *DFT* Molecular Dynamics simulation. It is clearly seen that a good agreement with an experiment was achieved.

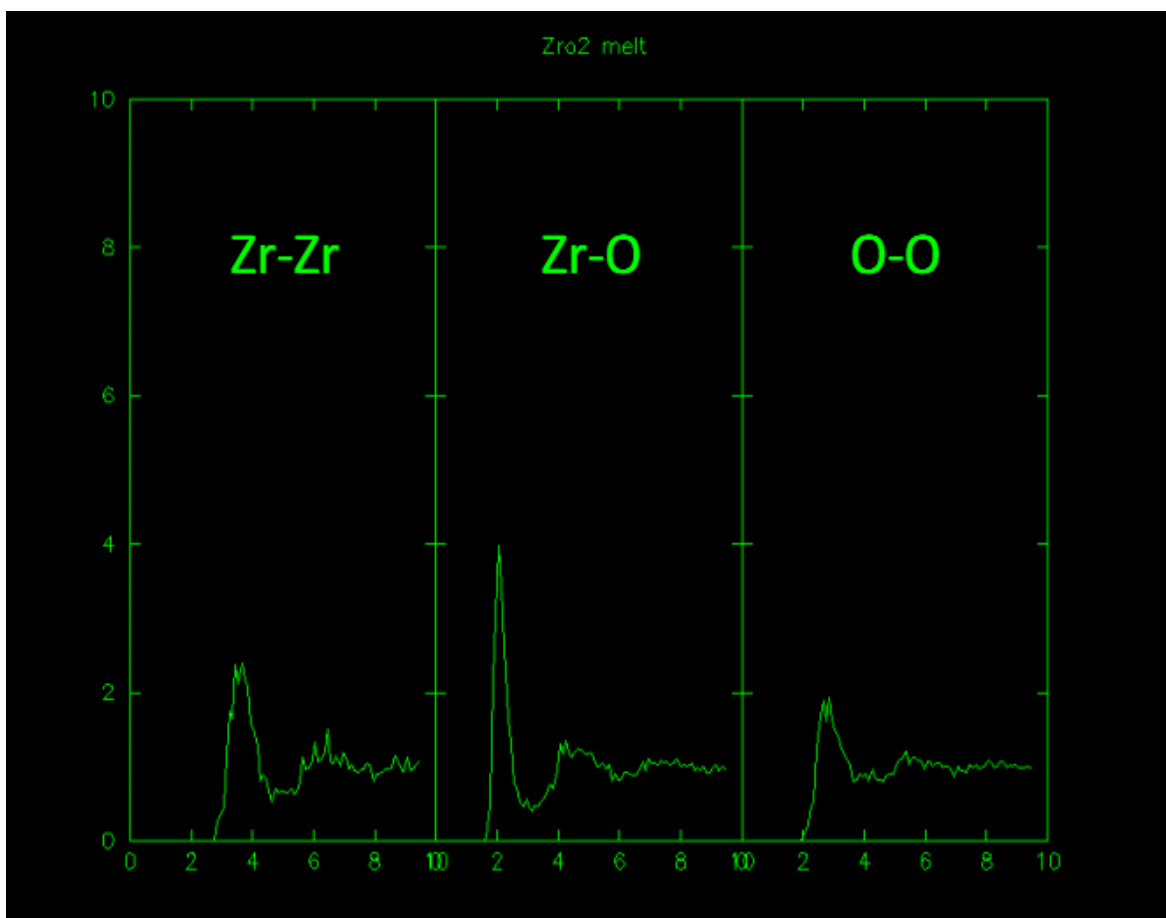


Figure 5. Partial distribution functions for atomic types Zr-Zr, Zr-O and O-O.

Partial distribution functions (figure 5) were calculated after the simulation to establish the most probable distances between each atomic type. Thereafter, we have calculated coordination numbers for each type of atomic (see table 1):

Table 1. Coordination numbers for ZrO₂ structure with the corresponding distance cut-offs.

Pair	Zr-O (2.8 Å)	O-Zr (2.8 Å)	Zr-Zr (4.6 Å)	O-O (3.8 Å)	O-O (2.8 Å)
CN	5.96	2.98	10.31	11.14	3.01

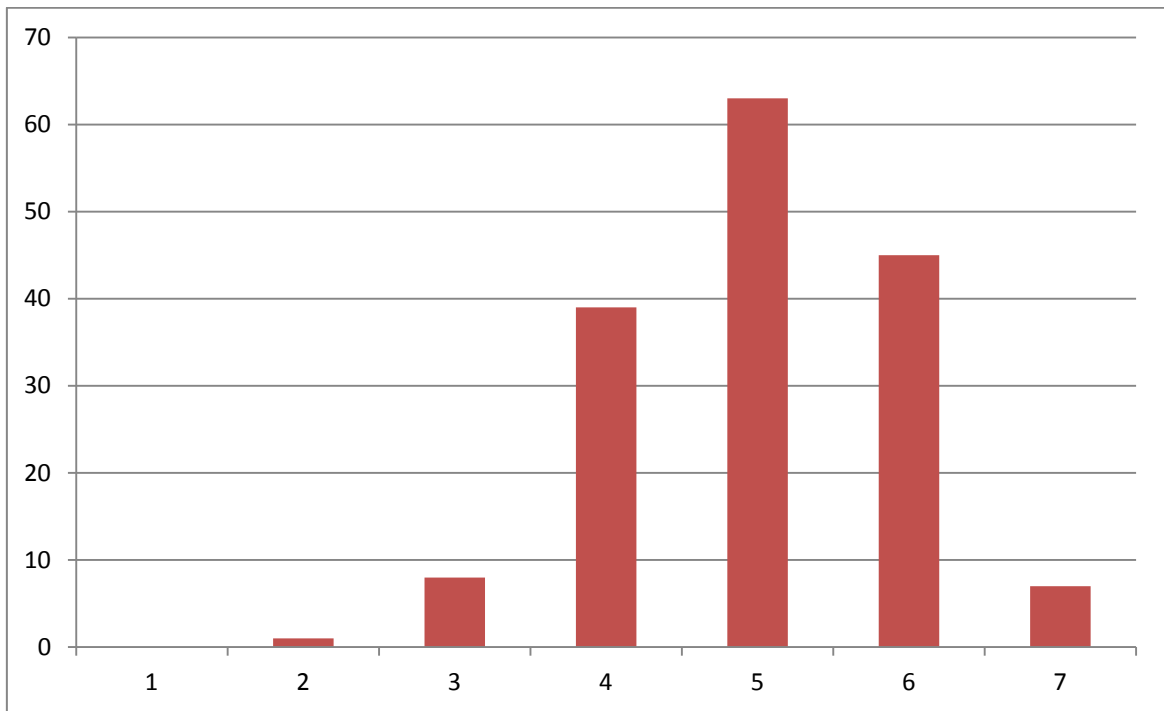


Figure 6. Distribution of coordination numbers for distances Zr-O.

Next, we have calculated distribution of coordination numbers for the first coordination sphere. As can be seen (figure 6), the most probable coordination numbers are 4, 5 and 6. Previous investigations of ZrO₂ have reported that the most probable coordination number for this structure equals to 7 [10]. The reduction of value for first coordination number can be simply explained by the temperature influence.

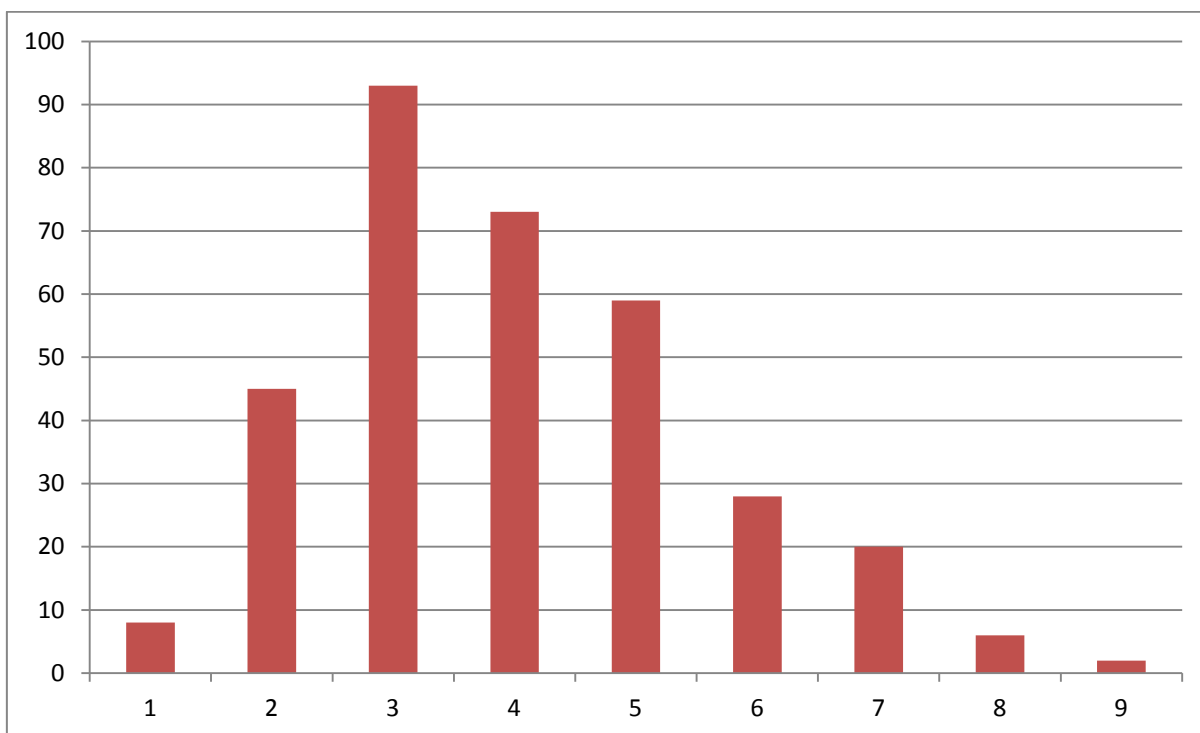


Figure 7. Distribution of coordination numbers for oxygen.

The distribution for coordination numbers is shown in figure 7. According to chemical formula, one Zr is associated with two O atoms. Therefore, the probable coordination number for oxygen should be in two times less than for Zr. In the article of D.Vanderbilt et al. [10] ‘Structural and dielectric properties of crystalline and amorphous ZrO₂’ the coordination number for O is equal to 3. Therefore, in our case for oxygen, the most probable coordination number corresponds to the previous investigation.

Thereafter, we have calculated projected density of states for each atomic type and evaluated the *HOMO-LUMO* gap.

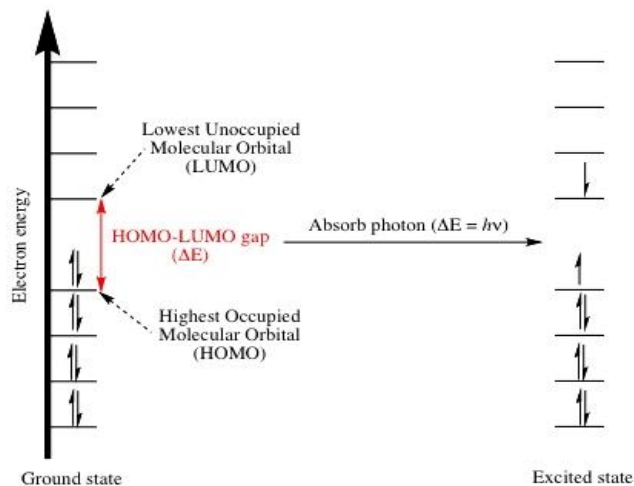


Figure 8. The energy difference between *HOMO* and *LUMO* orbitals is the *HOMO-LUMO* gap [11].

HOMO-LUMO gap (see figure 8) means the energy difference between a molecule's Highest-energy Occupied Molecular Orbital (*HOMO*) and its Lowest-energy Unoccupied Molecular Orbital (*LUMO*) [11]. During the simulation, *HOMO-LUMO* gap ($T = 3100$ K) is equal to 0.057 eV. Obviously, ZrO_2 is a semiconductor; therefore *HOMO-LUMO* gap for such materials should be more. But, our material was obtained under extreme temperature. It is liquid, and therefore it has a very small band gap.

Also, we performed Bader analysis to estimate effective charges. It is obvious (see table 3), that such small charges for Zr and O indicate covalent-type bonding between the atomic types.

Table 2. Average values for Bader and Voronoi charges.

Atomic type	Average value for Bader charge, in electrons	Average value for Voronoi charge, in electrons
Zr	$5.84 \cdot 10^{-2}$	$3.84 \cdot 10^{-2}$
O	$-1.59 \cdot 10^{-2}$	$-2.29 \cdot 10^{-2}$

In addition, we have calculated projected density of states for each atomic type (see figures 9, 10 and 11).

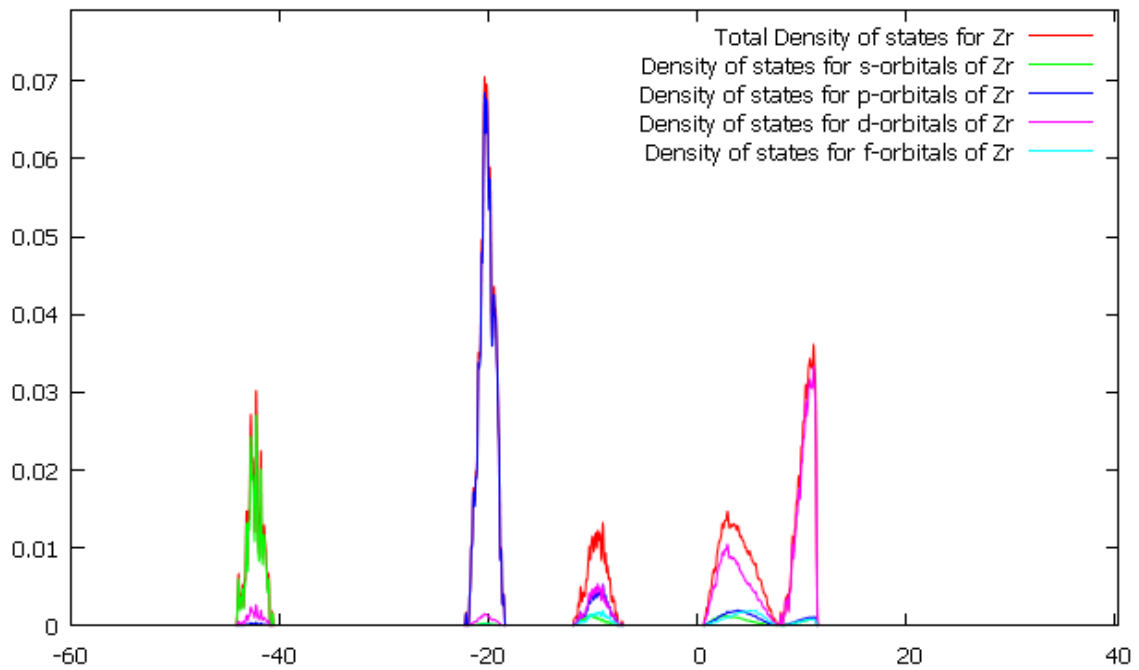


Figure 9. The total projected density of states for Zr and projections for each atomic orbital of Zr.

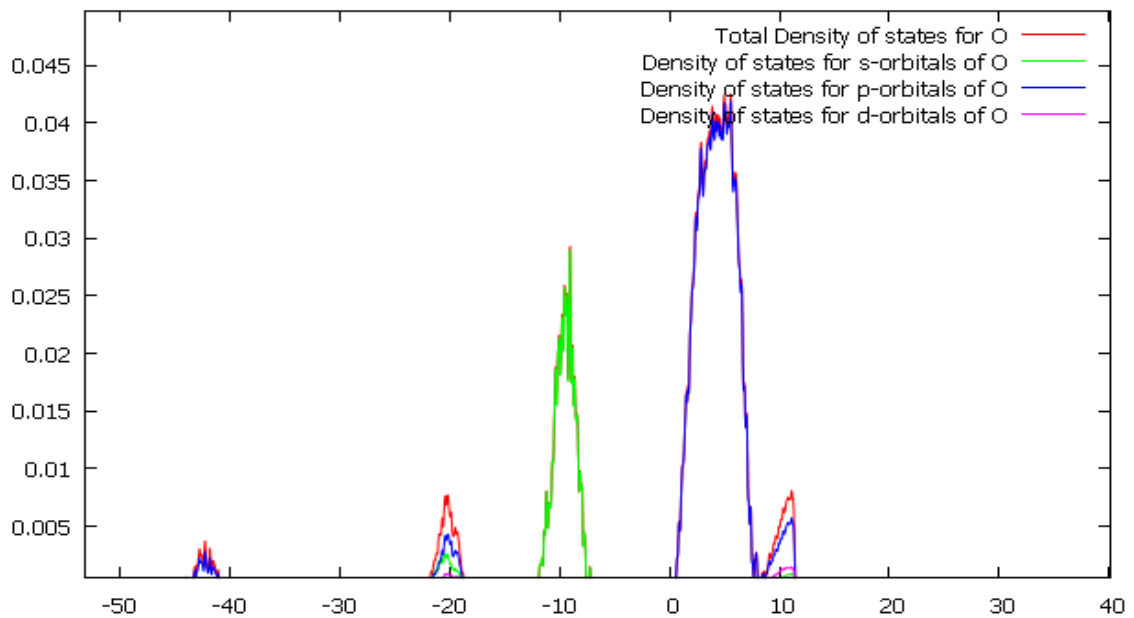


Figure 10. The total projected density of states for O and projections for each atomic orbital of O.

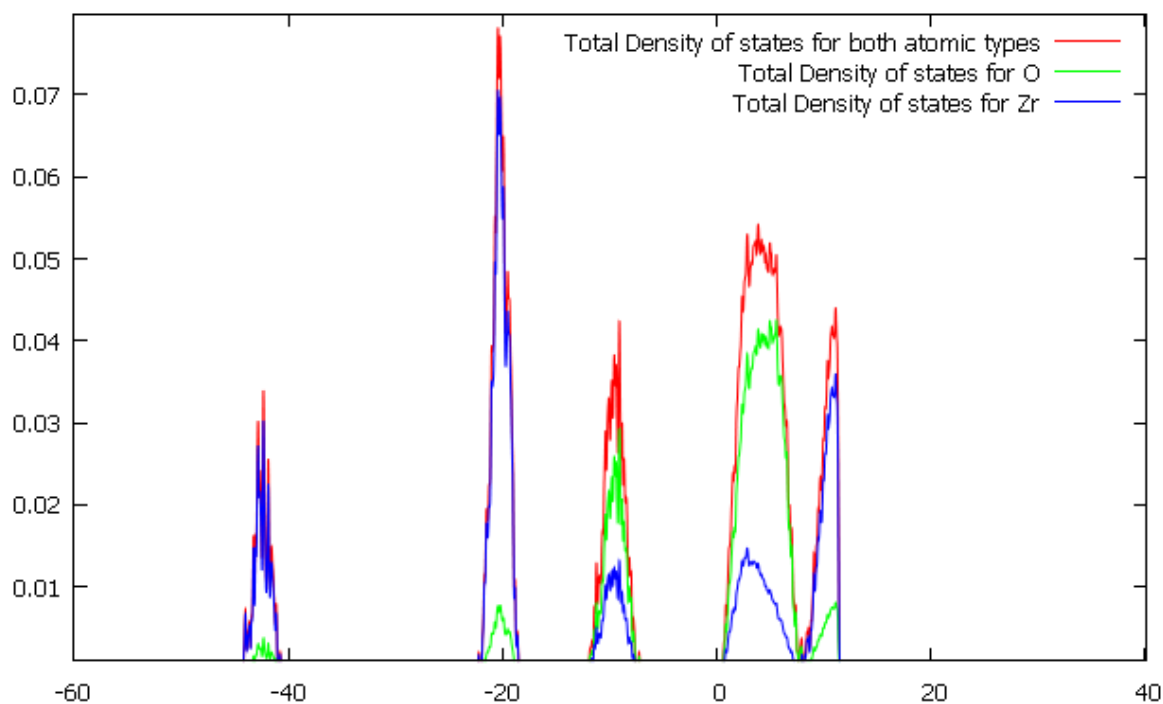


Figure 11. The red, green and blue curves represent the total density of states for both atomic types, O and Zr respectively.

Figures 11, 12 and 13 show, that the conduction band is composed mainly by p-electrons of oxygen and d-electrons of zirconium. The positions for the first peak (near to -40 eV) and for the second (near to -20 eV) peak are formed mainly by s- and p- valence electrons of Zr. This is an obvious result, since s- and d-orbitals have the lowest energy in comparison with the other valence orbitals. The position of each peak (figures 9, 10 and 11) can be verified, for example, by x-ray absorption spectroscopy.

Finally, we have calculated distribution for O-Zr-O and Zr-O-Zr (figures 12 and 13). The average values for angles are shown in table 3. It can be clearly seen, that average values for the angles are rather close to the characteristic angles for sp^2 and sp^3 hybridization types (109 and 120 angles respectively).

Table 3. Average values for angles.

Angle	Average value
O-Zr-O	105.277
Zr-O-Zr	118.548

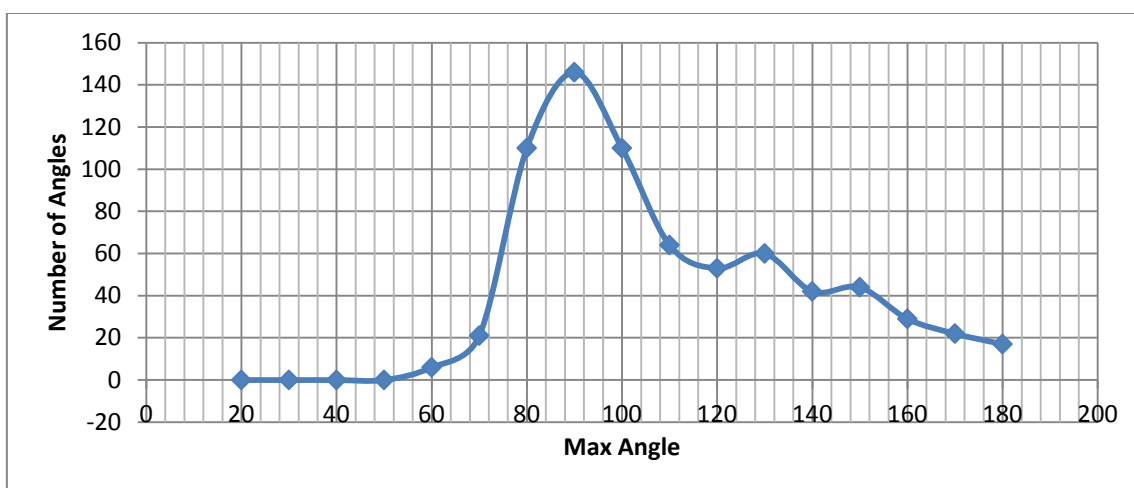


Figure 12. Distribution of O-Zr-O angles

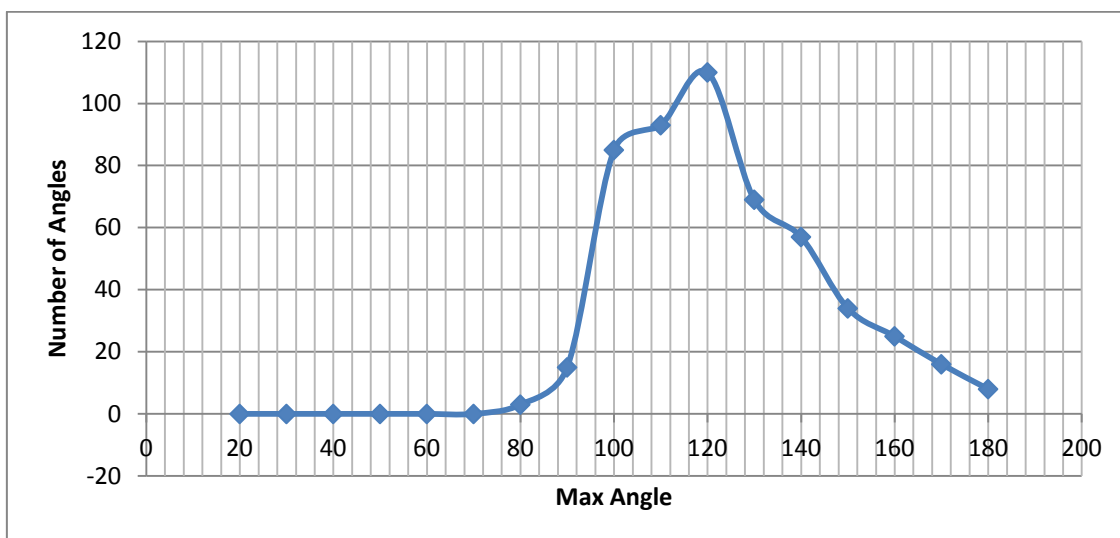


Figure 13. Distribution of Zr-O-Zr angles

Table 4. Diffusion coefficients of liquid ZrO_2 ($T = 3100$ K)

Atomic type	Total average value ($\text{\AA}^2/\text{fs}$):	Square of deviation ($\text{\AA}^4/\text{fs}^2$)	Standard deviation ($\text{\AA}^2/\text{fs}$):
Zr	$2.770 \cdot 10^{-5}$	$2.049 \cdot 10^{-12}$	$0.143 \cdot 10^{-5}$
O	$1.653 \cdot 10^{-4}$	$7.553 \cdot 10^{-11}$	$0.087 \cdot 10^{-4}$

As mentioned above, our system is liquid. We decided to calculate diffusion coefficients for both atomic types. These values should be compared with the corresponding values in the literature.

2.2.2 Atomic structure of ZrO_2 (CLASSICAL MD simulation)

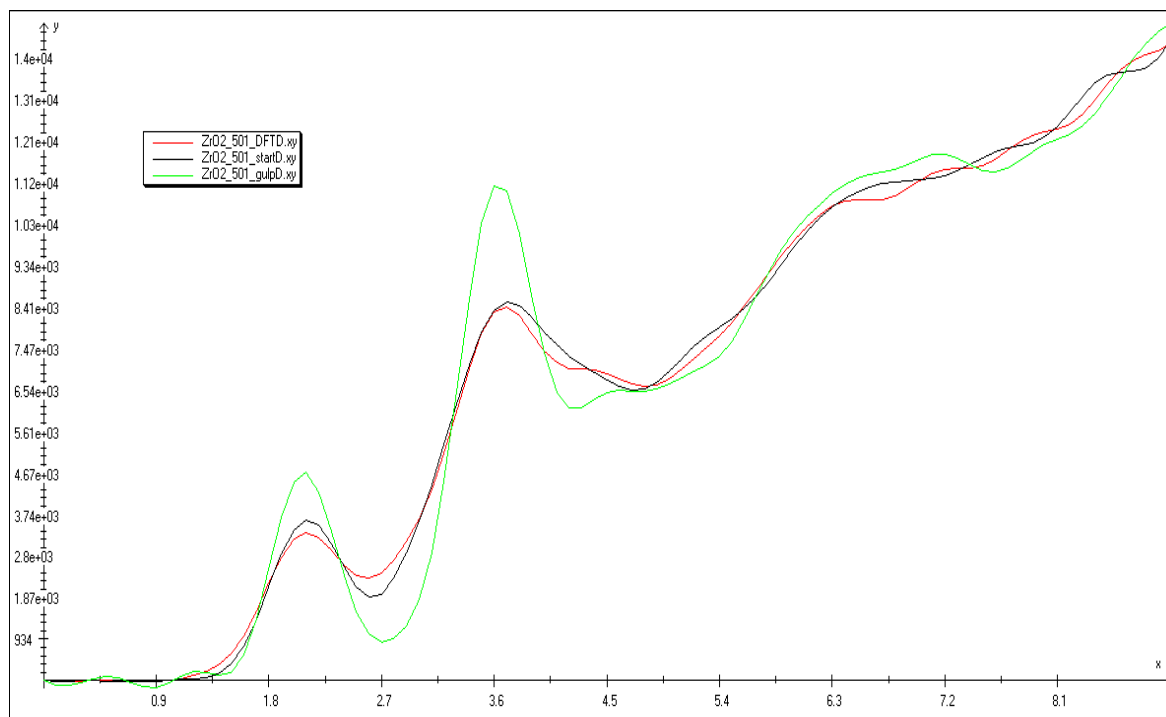


Figure 14. Total pair correlation functions. Red curve is the final configuration after *DFT* simulation, black curve is the initial configuration for ZrO_2 , and green curve corresponds to the final structure obtained after Classical *MD* simulation.

The classical molecular dynamic simulation was implemented using the program Gulp [12]; parameters for the simulation correspond to parameters for *DFT MD*. The total pair correlation function is shown in figure 14. Obviously, we have obtained more ordered structure (peak heights are greater, but the characteristic distances are the same as for the physical experiment, see figure 14), and therefore the accuracy of classical *MD* simulation is not enough to archive a good agreement with the physical X-Ray experiment.

2.3 Atomic structure of glassy B_2O_3

2.3.1 Ab initio MD simulation using initial configurations after RMC refinement

Currently, there is no consensus about the fractional number (f) for glassy structure of B_2O_3 [13-18]. Therefore, as mentioned above, the main purpose of this investigation is to establish the fractional number for boron.

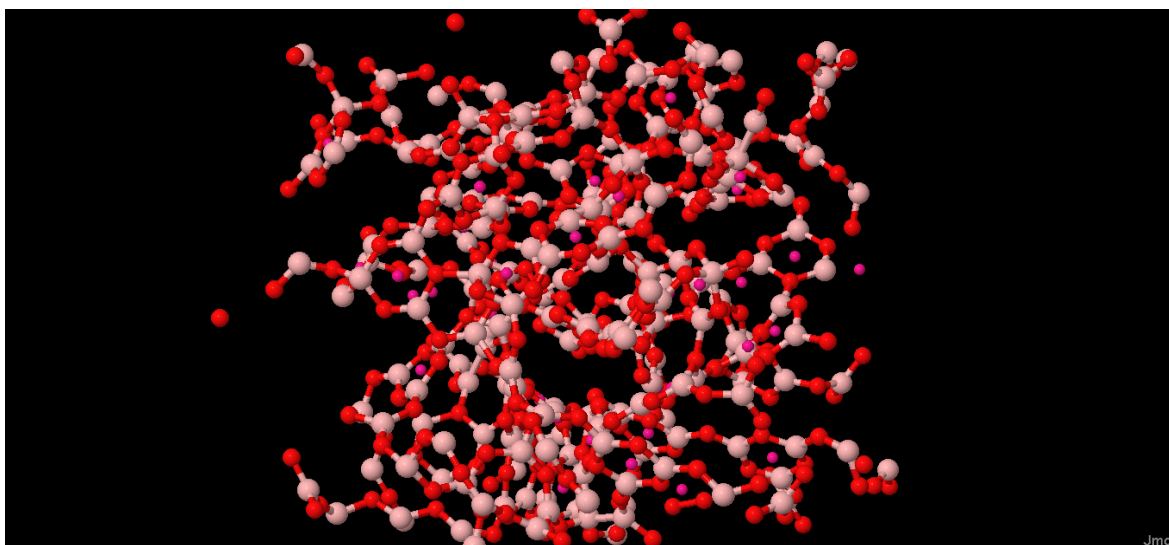


Figure 15. A glassy structure of diboron trioxide obtained after *DFT* simulation. The red, white and violet color represents oxygen, boron and dummy atoms, respectively. Dummy atoms are used to indicate a geometric center of a boroxol ring.

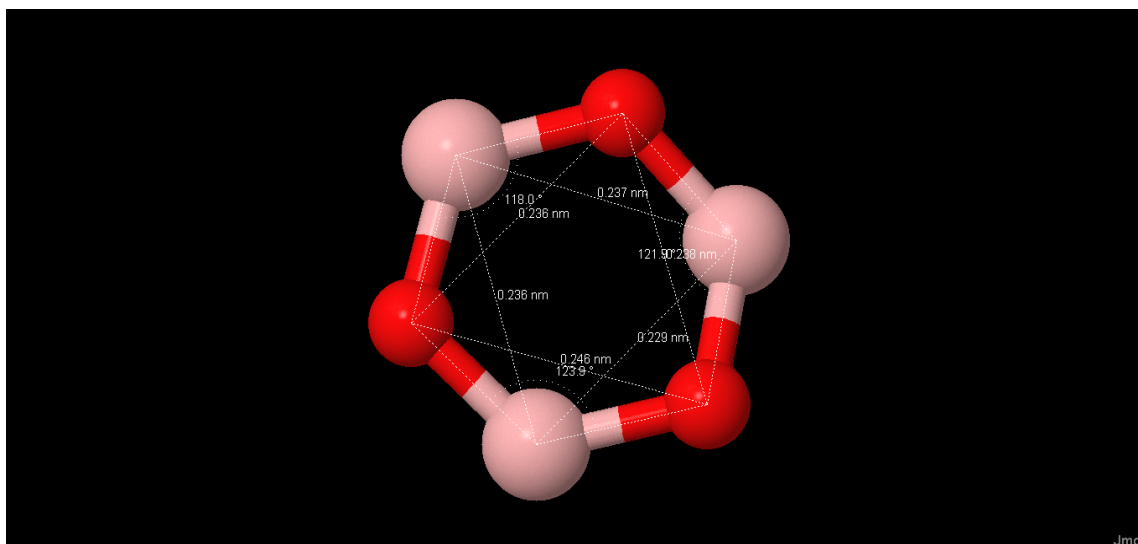


Figure 16. A typical boroxol ring for B_2O_3 structure.

As shown in figure 15, B_2O_3 is a glassy structure with an interesting short-range order. The coordination number for B is equal to 3 and the coordination number for O is equal to 2. Figure 16 shows a typical boroxol ring for B_2O_3 structure.

There are many results for the fractional number of boron in these rings. Data obtained by nuclear magnetic resonance method shows that the fractional number for this structure should be in the range from 65 to 85 %. But, on the other hand, previous studies by *DFT* methods shows that appropriate value for the fractional number should be less than 30 % [13-18].

For the first time, we implemented *DFT* simulation using the initial configuration which was obtained after *RMC* refinement method (x-ray diffraction data; Spring-8, Japan). We used *BFGS* method to optimize the geometry for the structure. Thereafter, we performed *DFT* Molecular Dynamic simulation. The time for the simulation was equal to 56 ps (the real time was approximately equal to 1 month using supercomputer in Espoo, CSC, with 64 cores). The Initial fractional number was equal to 54.29 %. After the simulation we have obtained the fractional number 55.71%.

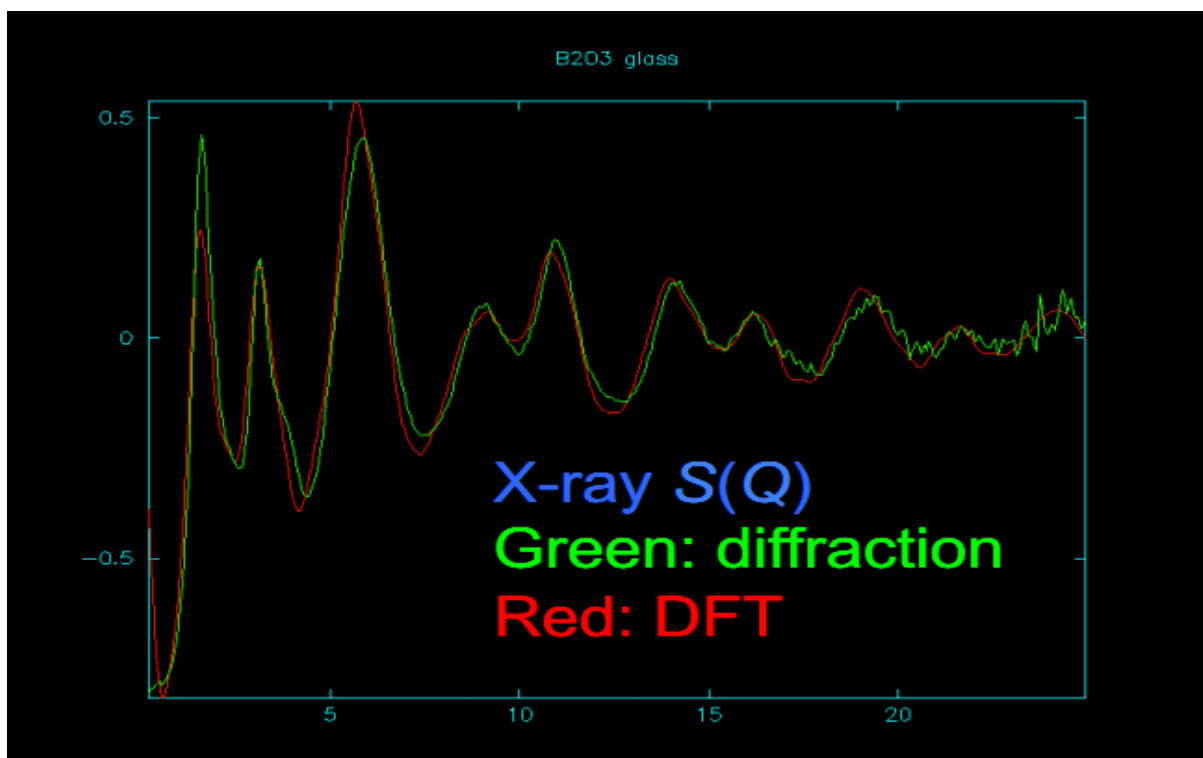


Figure 17. The Total structure factor of B_2O_3 . Red and Green curves represent structure factors for DFT simulation and physical experiment respectively.

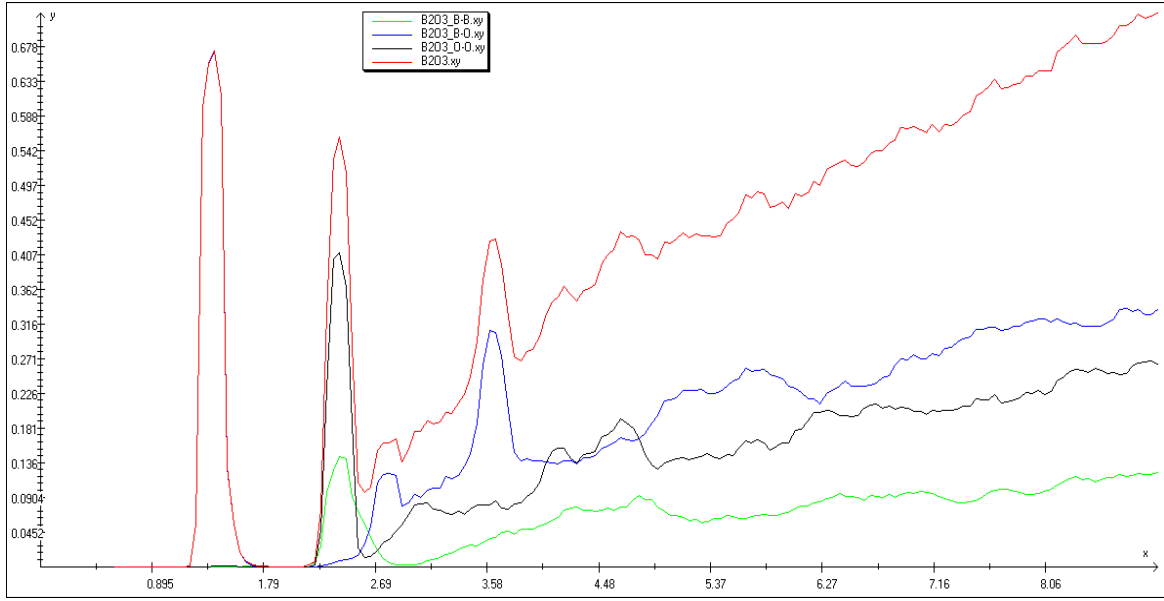


Figure 18. The total pair correlation (red curve) and partial pair correlations functions for B-B (green curve), O-O (black curve), and B-O (blue curve).

As can be clearly seen (figure 17), a good agreement between the *DFT* simulation and the physical experiment was obtained. Figure 18 represents pair functions for B_2O_3 structure. The first maximum of the total pair function ($\approx 1.38 \text{ \AA}$) is a distance between atomic types B and O. Partial correlation functions (figure 18) shows that the second maxima represents the nearest distances between B-B and O-O atoms.

Second time, when we used the boroxol-poor configuration, the fractional number was equal to 17.14%. After the simulation process (as previously, we used *BFGS* optimization method and 9 ps for *DFT MD* method) the fractional number was the same, as initially.

Direct *MD* simulation allows only short runs. For example, it is possible to perform *MD* simulation for 10 ps in the case of *ab initio MD* and for 10 ns in the case of Classical *MD*. However, many physical phenomena take place on a larger time scale: diffusion, phase transitions and etc [19]. In our case, this time is not enough for the formation of boroxol-rich structures. We conclude that the time scale that is used in the method of *DFT MD* is not enough for the formation of new boroxol rings. The maximum value f that could be achieved by *RMC* method was equal to 55 %. So, the main question was: “How to obtain a fractional number f more than 70 % and a good agreement with the physical experiment at the same time?”

2.3.2. Preparation of initial configurations by using classical MC method

As mentioned above, it was hard to prepare initial structures with f more than 55 % using only *RMC*. In order to create initial configurations it was decided to use Classical *MC* instead of *RMC* method. An appropriate program for this case was written during this investigation.

We have used the following idea for the *MC* modeling:

1. Use optimized rigid rings after *DFT* modeling.
2. Move and rotate rings respect to each other to minimize the potential energy for the system. In order to calculate the potential energy pair potentials have been used. [18]
3. Add other atoms (which do not belong to the rings) and minimize the potential energy again.

Moreover, we used the next restrictions:

- Minimal distance for each type of atom (see table 5).
- The rings were fully rigid, therefore, the destruction of the rings during to simulation was not possible.

Table 5. Minimal distances which were set for each type of atom. A dummy atom is just a geometry centre of a ring.

N	Atomic type 1	Atomic type 2	Distance between atoms, in Å
1	B	B	2.15
2	B	O	1.2
3	O	O	2.15
4	Du	Du	4.0

Thereafter, we prepared configurations with different fractional numbers in the range from 10 % to 80 %. After the end of Classical *MC* simulations, we calculated real number of rings. As can be seen (table 6), additional rings were formed during to classical simulation processes. Next, we prepared *BFGS* geometry optimization using *DFT* method. For each case the final energy after optimization process was approximately equal to -5666 Hartree units, in other words, the differences between initial (table 6) and final configurations was ≈ 1.04 eV/atom. That is why the fractional number after *DFT* simulation drops more than in 2 times after the geometry optimization process (table 7).

Table 6. The Initial configurations for *DFT* method.

expected number of rings	real number of rings	real fractional number for B after classical MC simulation,%	initial energy(classical MC), Hartree	energy(after MC), per atom, Hartree	energy per atom, eV
7	10	14.29	-5642.33	-10.747	-292.44
14	20	28.57	-5641.63	-10.745	-292.41
21	25	35.71	-5640.41	-10.743	-292.34
28	29	41.43	-5641.90	-10.746	-292.42
35	36	51.46	-5638.20	-10.739	-292.23
42	43	61.43	-5636.79	-10.736	-292.16
49	49	70.0	-5639.01	-10.740	-292.27
56	58	82.86	-5638.23	-10.739	-292.23

Table 7. The final values for fractional number obtained after optimization of geometry.

real number of rings	real fractional number after classical MC simulations,%	final number of rings after geometry optimization (BFGS, DFT)	final fractional number after geometry optimization process,%
10	14.29	9	12.86
20	28.57	9	12.86
25	35.71	20	28.57
29	41.43	21	30.00
36	51.46	14	20.0
43	61.43	24	34.29
49	70.0	17	24.29
58	82.86	30	42.86

2.3.3 Creation of initial configuration using both methods (RMC and Classical MC)

A decision was made to use a combination *RMC* and Classical *MC* methods to create initial configurations for *DFT* simulations. Classical *MC* method was used to generate boroxol-rich configurations with a fractional number more than 70 %, *RMC* method was used to provide the best agreement with the physical experiment. For *RMC* modeling we used rigid rings which were obtained after *MC* modeling.

For the first time, we used an initial structure which was obtained by using *RMC* and *MC* methods with the fractional number 82.86 %. We have estimated the total energy for our structure after *DFT* simulation. The energy difference between the initial (after classical *MC* and *RMC* methods) and the final structure (after *DFT* method) was only 0.26 eV/atom, thereby avoiding large structural rearrangements. After *DFT* simulation (*BFGS* method + *MD* method) we calculated the fractional number for the structure, it was equal to 64.29 %. As discussed in the chapter 2.3.1, a fractional number remains constant for initial structures obtained by *RMC* method. But, in the last simulation the fractional number was reduced. The reduction of the fractional number is additional evidence that the ‘saturation level’ for f should be close to 70 percent.

Thereafter, we performed new configurations using both methods with fractional numbers 96 and 97 percents. *BFGS* geometry optimizations were performed for both structures. After the optimization process, the fractional number for the first structure reduced from 97 to 61.4 percent. We performed a short *MD* run, after the simulation the fractional number dropped from 61.4 to 54.29%. For the second structure, the fractional number decreased from 96 to 71.4 percent after the *BFGS* geometry optimization method and *DFT* molecular dynamic simulation with the duration of 22 ps. Therefore, we can conclude that the ‘saturation level’ for f should be in the range between 70 and 75%. Therefore, it was shown that it is possible to obtain an agreement for fractional number between *NMR* and *DFT* techniques using suitable initial configurations.

2.3.4 Projected density of states for boroxol-rich B_2O_3 structure.

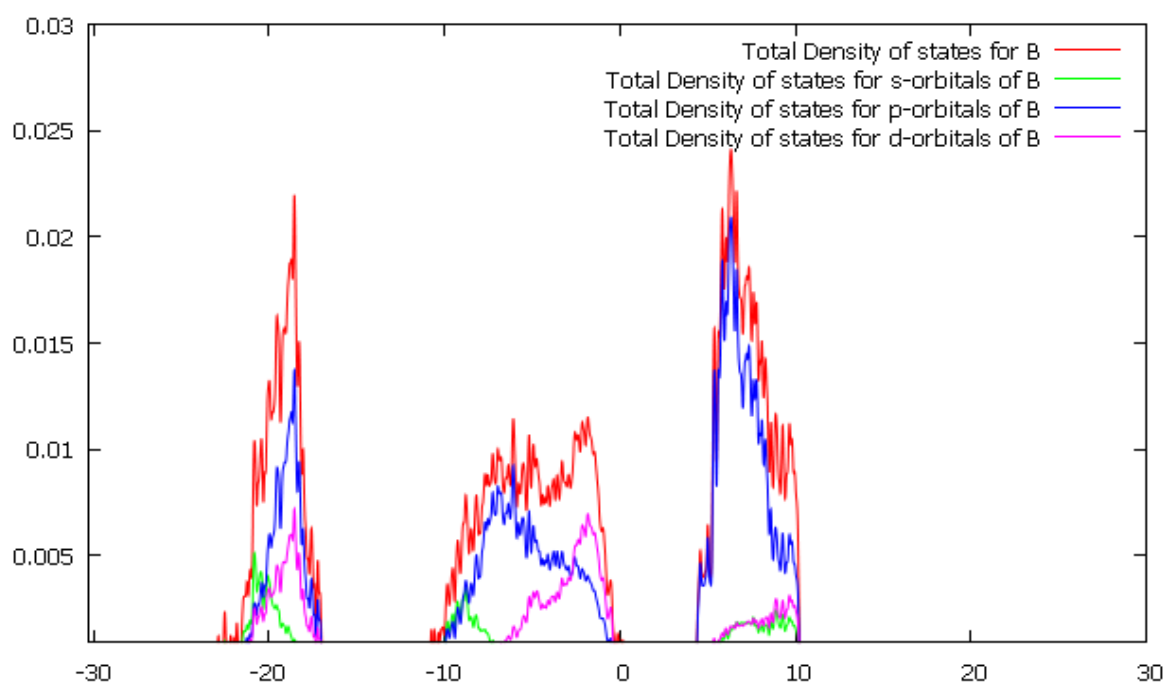


Figure 19. The total projected density of states for B (red curve) and projections for each atomic orbital of B.

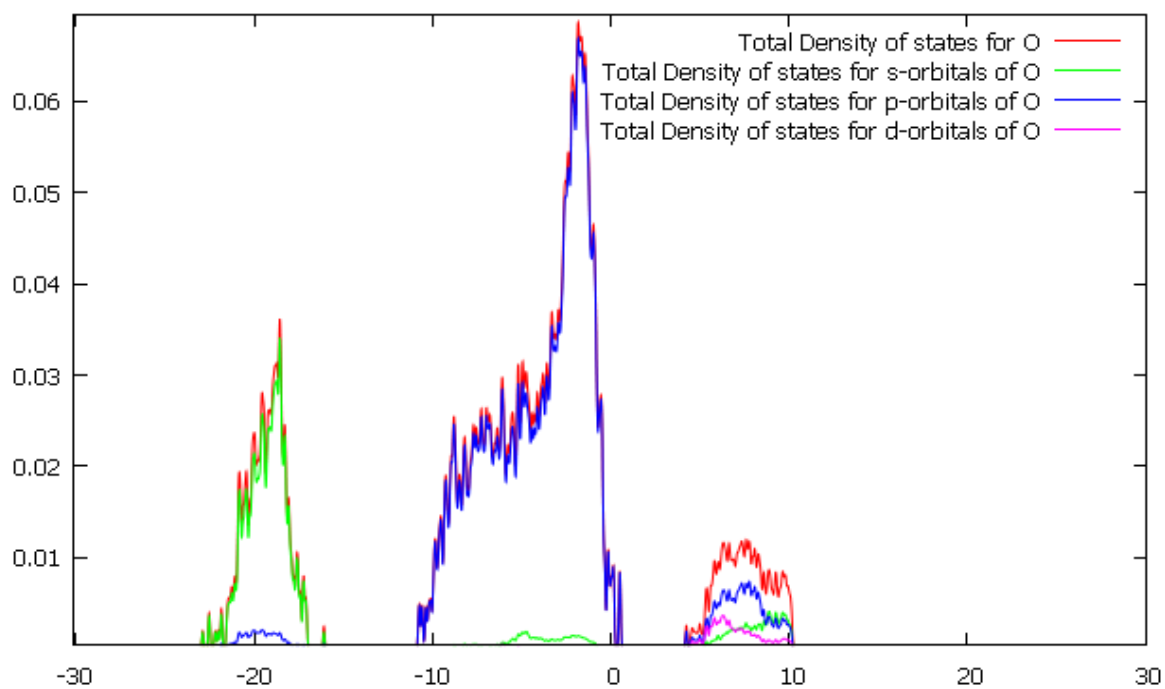


Figure 20. The total projected density of states for O (red curve) and projections for each atomic orbital of O.

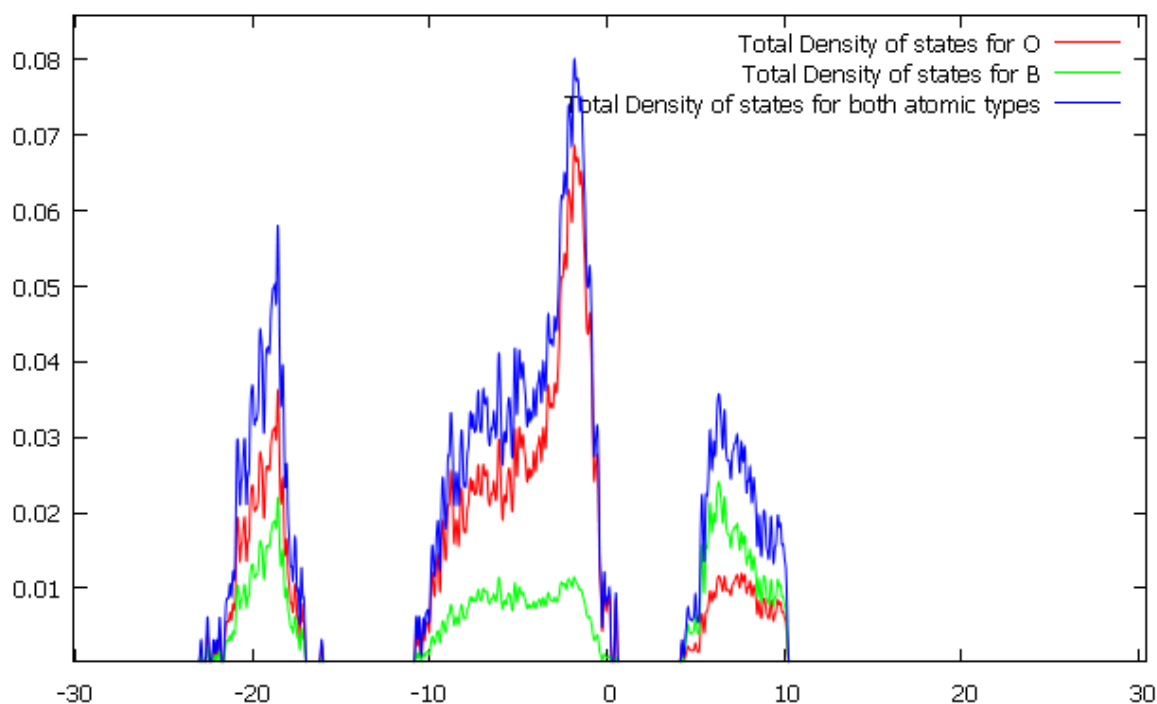


Figure 21. Blue, green and red curves represent the total density of states for both atomic types, B and O respectively.

In the end simulation, we have implemented *PDOS* calculations using *DFT* techniques. The Fermi energy for a given system is equal to 0.534 eV. The conduction band is mostly composed by p-orbitals of B. One can notice that the difference between the valence and conduction bands is ≈ 3 eV. Therefore, the given structure can be treated as a wide gap semiconductor. In order to verify the data of *PDOS*, data of physical experiments can be used (for example, the data of x-ray absorption spectroscopy (*XAS*)).

2.3.5. Comparison between boroxol-rich and boroxol-poor structures.

In summary, we consider the difference between boroxol-poor (f is equal to 17.1; *BFGS* optimization method and *DFT MD* simulation with duration of 9 ps) and boroxol-rich structures (f is equal to 71.4; *BFGS* method + 22 ps for *ab initio* molecular dynamic simulation).

As was mentioned above, both structures have a good agreement with the physical experiment (x-ray diffraction). Projected densities of states were calculated for both cases (figures 22 and 23).

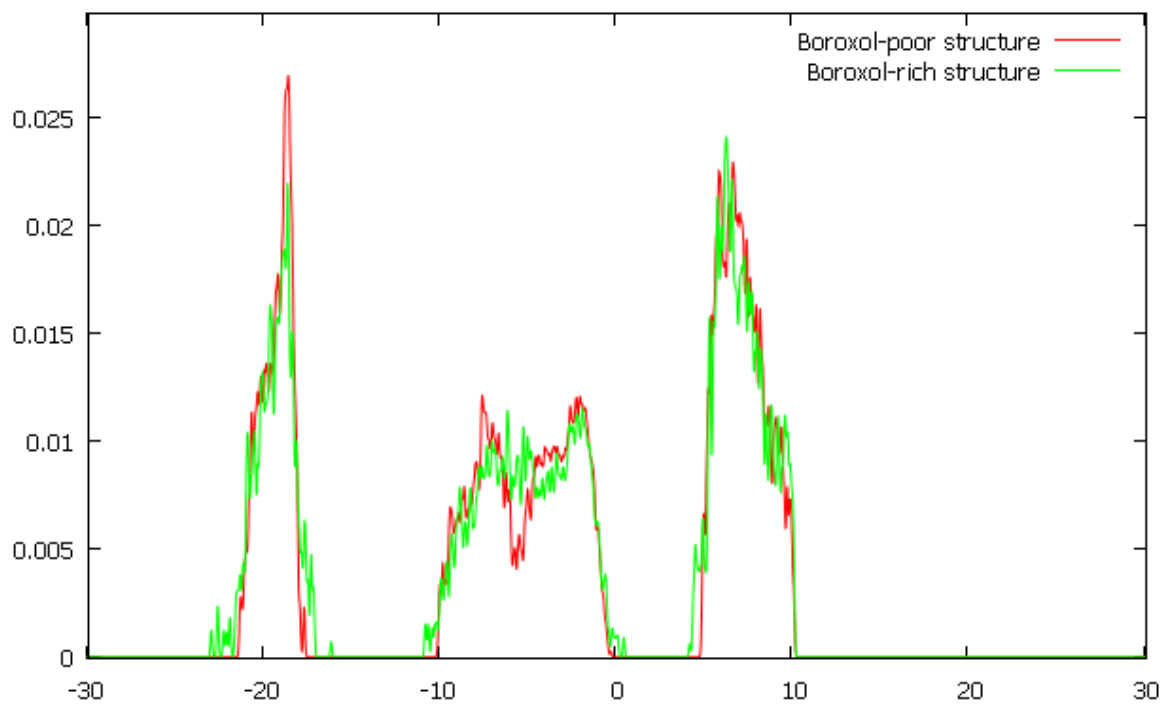


Figure 22. The projected density of states of boron. The comparison between boroxol-poor and boroxol-rich structures.

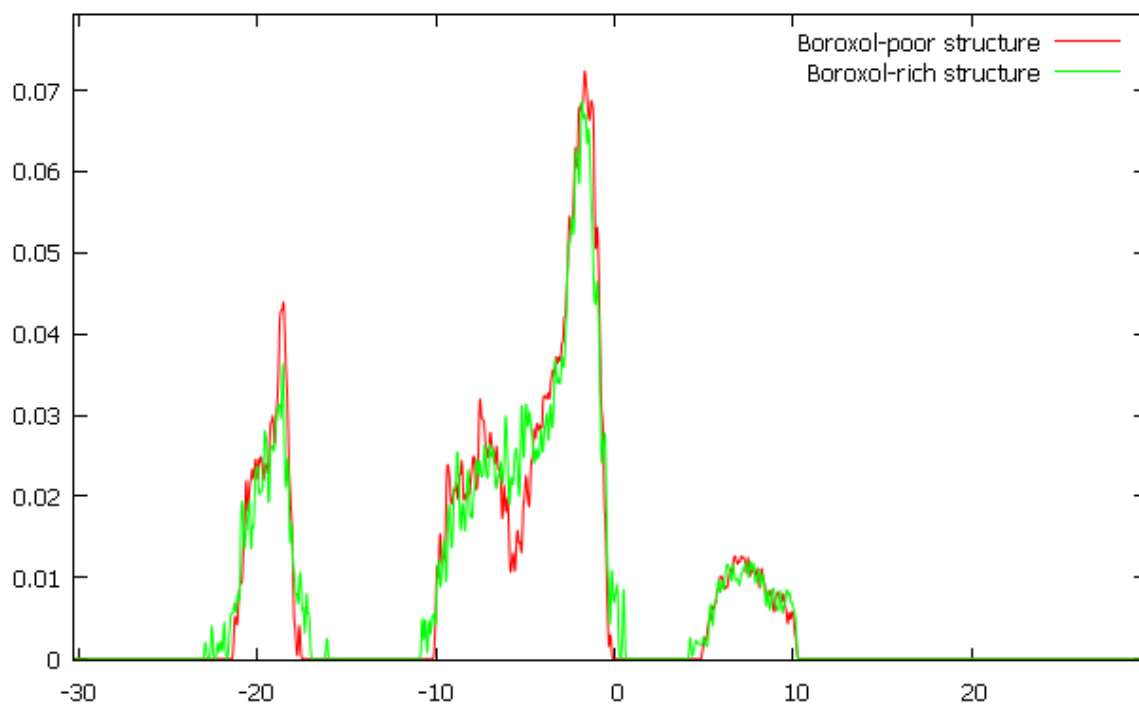


Figure 23. The projected density of states of oxygen. The comparison between boroxol- poor and boroxol-rich structures.

Table 8. Comparison of potential energies for boroxol-poor and boroxol-rich structures.

Name	fractional number, %	Potential energy after the DFT simulation, Hartree
boroxol- poor structure	17.1	-5666.697
boroxol- rich structure	71.4	-5666.956

Table 9. HOMO-LUMO gap and Fermi energies for boroxol-poor and boroxol-rich structures.

Name	fractional number, %	HOMO-LUMO gap, eV	Fermi Energy, eV
boroxol- poor structure	17.1	5.189	-0.224
boroxol- rich structure	71.4	3.722	0.534

As shown in figures 22 and 23, there is no considerable difference in the densities of states between boroxol- poor and boroxol-rich structures.

In the end of simulations we calculated the *HOMO-LUMO* gap, Fermi energy (table 9) and potential energy (table 8) for both cases. As can be clearly seen from the table 8, the potential energy is lower in the case of the boroxol-rich structure; it is an additional proof that the valid value for the fractional number is closer to 70 percent.

Conclusion

1. We have investigated the structure and dynamics of ZrO_2 under extreme conditions ($T = 3100 \text{ K}$). In order, to describe the structure, coordination spheres, pair functions, structure factors, characteristic angles and diffusion coefficients were calculated for the given temperature. Currently, there is no information about structure of ZrO_2 at such high temperatures. Therefore, our investigation can be considered as a new. The atomic model which is obtained during to *DFT* simulation has a perfect agreement with the physical X-Ray experiment.

2. Characteristic times for simulations by *DFT* method is usually a few tens of picoseconds. This time is not enough for the formation of boroxol-rich structures. Thus, there is a large difference between data for f of *NRM* and *DFT* methods (f is equal to 0.3 for *DFT* methods and f is equal to 0.7 in the case of *NMR*). We were able to show that this difference can be eliminated by creating an appropriate initial configuration for glassy structure of B_2O_3 . On the one hand, we should obtain fractional number for B more than 70%. On the other hand, the total energy for an initial configuration should be close to the minima for *DFT* simulation to avoid the destruction of boroxol rings. As shown above, it can be achieved by using the combination of classical *MC* and *RMC* methods. At the present time, there is no consensus in the literature about the fractional number for B between *DFT* and *NMR* techniques; therefore we have solved this problem. We have made a new contribution for glassy structure of B_2O_3 .

References

- [1] Nekrasov. I.A. (2012). Modern methods for electronic structure calculations using LDA and LDA+DFMT approximations, Russian Academy of Science, Electrotechnical Institute URO, RAN. [online document] [Accessed April 20 2012]. Available at http://sadowski.iep.uran.ru/RUSSIAN/LTF/dynasty_school.html.
- [2] Marx D. and Hutter J. (2000). Ab Initio Molecular Dynamic: Theory and implementation. John Von Neuman Institute for Computing. [online document]. [Accessed 3 June 2012]. Available at <http://www2.fz-juelich.de/nic-series/Volume3/marx.pdf>.
- [3] Kohanoff J. (2006). Electronic Structure Calculations for Solids and Molecules: Theory and Computational Methods, Cambridge University Press.
- [4] Mc Greevy R.L. (2001). Reverse Monte Carlo. Topical review. J.Phys. Condens. Matter 13, R877.
- [5] Dove. M.T. (2009). An Introduction to atomistic simulations methods. Seminars de la SEM, Vol.4, 7-37.
- [6] Allen. M.P. (2004). Introduction to Molecular Dynamics Simulation. John von Neumann Institute for Computing, [online document]. [Accessed 17 June 2012]. Available at <http://www2.fz-juelich.de/nic-series/volume23/allen.pdf>
- [7] CP2K input reference. (2012). [Accessed April 15 2012]. Available at <http://manual.cp2k.org/trunk/index.html>.
- [8] A C++ implementation of the Reverse Monte Carlo algorithm. [online document]. [Accessed April 2012]. Available at <http://www.szfki.hu/~nphys/rmc++/opening.html>
- [9] Finnish IT CENTER FOR SCIENCE. (2012). [online document]. [Accessed April 15 2012]. Information about CSC available at <http://www.csc.fi/english>
- [10] Vanderblit D., Zhao X., Ceresoli D. (2005). Structural and dielectric properties of crystalline and amorphous ZrO₂. The Solid Films 486, 125-128.
- [11] Organic Chemistry at UCLA. [online document]. [Accessed April 17 2012]. Available at http://www.chem.ucla.edu/harding/IGOC/H/homo_lumo_gap.html

- [12] Gale. J.D. (2012). Gulp manual. [Accessed April 10 2012]. Available at http://projects.ivec.org/gulp/help/gulp_30_manual/index.html .
- [13] Ferlat G, Charpentier T, Seitsonen AP, Takada A, Lazzeri M, Cormier L, Calas G, Mauri F. (2008). Boroxol Rings in Liquid and Vitreous B₂O₃ from First Principles. *Phys. Rev. Lett.* 101, 065504.
- [14] Umari P. and Pasquarello A. (2005). Fraction of Boroxol Rings in Vitreous Boron Oxide from a First-Principles Analysis of Raman and NMR Spectra, *Phys. Rev. Lett.* 95, 137401.
- [15] Soper A. K. (2011). Boroxol rings from diffraction data on vitreous boron trioxide. *J. Phys.: Condens. Matter* 23, 365402.
- [16] Youngman R. E. ,Haubrich S. T. , Zwanziger J. W. , Janicke M. T. and Chmelka B. F. (1995). Short-and Intermediate-Range Structural Ordering in Glassy Boron Oxide. *J. Science* ,Vol. 269 no. 5229 ,1416-1420.
- [17] Brazhkin V.V. , Katayama Y., Trachenko K. ,Tsiok O.B. ,Lyapin A.G., Artacho E., Dove M., Ferlat G., Inamura Y., Saitoh H. (2008). Nature of Structural Transformations in the B₂O₃ Glass under High Pressure, *Phys. Rev. Lett*, 101 (3). 035702-4.
- [18] Takada A., Catlow C.R.A. and Price G.D. (1995). Computer modelling of B₂O₃. New interatomic potentials, crystalline phases and predicted polymorphs. *J.Phys.:Condens.Matter* 7, 8659 .
- [19] Parrinello M. (2012). Ab Initio Molecular Dynamic, ETH Zurich, Physical Chemistry [online document]. [Accessed May 5 2012]. Available at <http://www.imprs-am.mpg.de/parrinello.pdf>
- [20] Sayan S. , Nguyen N. V. , Ehrstein J. , Emge T. , Garfunkel E. , Croft M., Zhao X. , Vanderbilt D. , Levin I. , Gusev E. P. , Hyounsub K, and McIntyre P. J. (2005). Structural, electronic, and dielectric properties of ultrathin zirconia films on silicon, *Appl. Phys. Lett.* 86, 152902.
- [21] Wang H., Lin K., (1991). Preparation and characterization of alkoxy-derived metastable cubic ZrO₂ powders. *Materials Science and Engineering: Vol. 147, Issue 2, 249–255.*

- [22] Dove M.T., Tucker M.T., Wells S.A., Keen D.A. (2002). Reverse Monte Carlo, EMU notes in Mineralogy, Vol. 4, Ch. 4, 59-82.
- [23] Probert M. and Hopkinson A. (2012). Bader Charge Analysis. [online document]. [Accessed April 2012]. Available at <http://theory.cm.utexas.edu/bader/>.
- [24] Tang W., Sanville E., and Henkelman G. (2009). A grid-based Bader analysis algorithm without lattice bias. J. Phys. Condens. Matter 21, 084204.
- [25] Sanville E., Kenny S. D., Smith R., and Henkelman G. (2007). An improved grid-based algorithm for Bader charge allocation. J. Comp. Chem. 28, 899-908.
- [26] Henkelman G., Arnaldsson A., and Jónsson H., (2006). A fast and robust algorithm for Bader decomposition of charge density. Comput. Mater. Sci. 36, 254-360.
- [27] Shinoda W., Okazaki S. (1998). A Voronoi analysis of lipid area fluctuation in a bilayer. The Journal of Chemical Physics, Vol. 109, No. 4. 1517-1521.
- [28] Ceresoli D. and Vanderbilt D. (2006). Structural and dielectric properties of amorphous ZrO_2 and HfO_2 . Phys. Rev. B 74, 125108

Appendix 1. The input file for the cp2k program. Ab initio MD simulation of glassy B₂O₃ structure (Microcanonical ensemble).

```
&FORCE_EVAL
METHOD Quickstep
&DFT
CHARGE 0
&MGRID
  CUTOFF 200
&END MGRID
&QS
  EPS_DEFAULT 1.0E-10
&END QS
&SCF
  SCF_GUESS RESTART
  EPS_SCF 1.0E-5
  MAX_SCF 100
  &OUTER_SCF
    EPS_SCF 1.0E-5
    MAX_SCF 80
  &END
&OT
  PRECONDITIONER FULL_ALL
&END
&END SCF
&XC
  &XC_FUNCTIONAL PBE
&END XC_FUNCTIONAL
```

```

&END XC
&END DFT
&SUBSYS
  &CELL
    ABC 18.655354 18.655354 18.655354
  &END CELL
  &COORD
! An array of atomic coordinates
  &END COORD
  &KIND O
    BASIS_SET DZVP-MOLOPT-SR-GTH
    POTENTIAL GTH-PBE-q6
  &END KIND
  &KIND B
    BASIS_SET DZVP-MOLOPT-SR-GTH-q3
    POTENTIAL GTH-PBE-q3
  &END KIND
&END SUBSYS
&END FORCE_EVAL
&GLOBAL
  PROJECT B2O3-525_96perc
  WALLTIME 86400
  RUN_TYPE MD
  PRINT_LEVEL LOW
&END GLOBAL
&MOTION
  &MD
    ENSEMBLE NVE
    STEPS 5000

```

```
TEMPERATURE 300.0
TEMP_TOL 25.0
TIMESTEP 2
&END
&END MOTION
&EXT_RESTART
  RESTART_FILE_NAME B2O3-525_96perc-1.restart
  RESTART_DEFAULT T
&END EXT_RESTART
```

Appendix 2. The input file for the cp2k program. Ab initio MD simulation of liquid ZrO₂ structure (Canonical ensemble).

```
&FORCE_EVAL
METHOD Quickstep
&DFT
  CHARGE 0
  &MGRID
    CUTOFF 240
  &END MGRID
  &QS
    EPS_DEFAULT 1.0E-10
  &END QS
  &SCF
    SCF_GUESS ATOMIC
    EPS_SCF 1.0E-5
    MAX_SCF 60
    &OUTER_SCF
      EPS_SCF 1.0E-5
      MAX_SCF 40
    &END
  &OT
    PRECONDITIONER FULL_ALL
  &END
&END SCF
&XC
  &XC_FUNCTIONAL PBE
  &END XC_FUNCTIONAL
&END XC
```

```

&END DFT
&SUBSYS
  &CELL
    ABC 18.977744 18.977744 18.977744
  &END CELL
  &COORD
! An array of atomic coordinates
  &END COORD
  &KIND O
    BASIS_SET DZVP-MOLOPT-SR-GTH
    POTENTIAL GTH-PBE-q6
  &END KIND
  &KIND Zr
    BASIS_SET DZVP-MOLOPT-SR-GTH-q12
    POTENTIAL GTH-PBE-q12
  &END KIND
&END SUBSYS
&END FORCE_EVAL

&GLOBAL
PROJECT ZrO2-501
WALLTIME 86400
RUN_TYPE MD
PRINT_LEVEL LOW
&END GLOBAL

&MOTION
&MD
ENSEMBLE NVT

```

STEPS 10000
TEMPERATURE 3100.0
Timestep 2

&THERMOSTAT

&NOSE

LENGTH 2

YOSHIDA 3

TIMECON 10000.0

MTS 2

&END NOSE

&END THERMOSTAT

&END

&END MOTION

&EXT_RESTART

RESTART_FILE_NAME ZrO2-501-1.restart

RESTART_DEFAULT T

&END EXT_RESTART